

Non-Line-of-Sight Ultraviolet Positioning Using Linearly-Arrayed Photon-Counting Receivers

Renzhi Yuan^{ID}, Member, IEEE, Siming Wang^{ID}, Gang Liu^{ID}, and Mugen Peng^{ID}, Fellow, IEEE

Abstract—Traditional optical positioning techniques employing visible light signals or infrared light signals require line-of-sight links between transmitters and receivers. The wireless positioning techniques using ultraviolet (UV) signals can enjoy both non-line-of-sight (NLOS) positioning ability and immunity to electromagnetic jamming. In this work, we focus on NLOS UV positioning techniques using linearly-arrayed photon-counting receivers. We first derive the geometrical and physical constraints for the NLOS UV positioning using linearly-arrayed receivers. We then derive the analytical relation between location parameters and pointing parameters of unknown transmitter and propose a NLOS UV positioning method with acceptable computational complexity. We further derive the Cramér-Rao bounds for the positioning method when the separate distance between adjacent receivers equals zero. Numerical results demonstrate that the proposed NLOS UV positioning methods using photon-counting receivers can achieve a distance error less than 2 m when the transmitting elevation angle is greater than 30 degrees and the separate distance is greater than 2 m. Besides, we demonstrate that at least three receivers are required to avoid multiple solution problem; and three receivers are enough for achieving an acceptable positioning error for NLOS UV positioning using photon-counting receivers.

Index Terms—Non-line-of-sight, photon-counting receivers, ultraviolet positioning.

I. INTRODUCTION

A. Background and Motivations

OPTICAL positioning techniques [1], [2], [3] enjoy advantages such as high positioning precision, low costs, and immunity to electromagnetic jamming compared with other wireless positioning techniques using radio-frequency (RF) electromagnetic waves [4], [5], [6], [7], [8]. Traditional optical positioning techniques usually adopt visible light signals or infrared light signals as information carriers, which require line-of-sight links between the target source and the signal receivers and thus greatly restrict the applications of optical

Manuscript received 14 November 2023; revised 18 March 2024; accepted 9 May 2024. Date of publication 13 June 2024; date of current version 21 August 2024. This work was supported in part by the National Key Research and Development Program of China under Grant 2021YFB2900200, in part by the National Natural Science Foundation of China under Grant 62201075 and Grant 61925101, in part by Beijing Natural Science Foundation under Grant L223007, and in part by Beijing Municipal Science and Technology Project under Grant Z211100004421017. (*Corresponding author: Renzhi Yuan*)

The authors are with the State Key Laboratory of Networking and Switching Technology, Beijing University of Posts and Telecommunications, Beijing 100876, China (e-mail: renzhi.yuan@bupt.edu.cn; wangsiming@bupt.edu.cn; rothony@bupt.edu.cn; pmg@bupt.edu.cn).

Color versions of one or more figures in this article are available at <https://doi.org/10.1109/JSAC.2024.3413960>.

Digital Object Identifier 10.1109/JSAC.2024.3413960

positioning techniques. Though RF based wireless positioning techniques can achieve non-line-of-sight (NLOS) positioning, they are vulnerable to the electromagnetic jamming. Therefore, it is necessary to seek for novel wireless positioning methods enjoying both ability of NLOS positioning and immunity to electromagnetic jamming.

Due to the strong scattering effect in the atmosphere, the ultraviolet (UV) signals in “solar-blind” waveband can establish NLOS links between the transmitter and the receiver [9], [10], [11]. Apart from the inherent immunity to electromagnetic jamming, the strong absorption effect of UV signals in the atmosphere can further guarantee good local security for information exchanging links using UV signals [12]. Besides, the UV links also enjoys low background noise due to the fact that the background solar radiation in the UV waveband has been strongly absorbed by the Ozone layer of the atmosphere [9], [10], [11]. Thanks to these inherent advantages, the NLOS UV communication becomes a promising option for both military communications under electromagnetic shielding scenarios and civil communications under electromagnetic sensitive environments¹ [16].

The NLOS UV communication has been elaborately researched in existing literatures [9], [10], and [11]. For example, the single-scattering [17], [18], [19], [20] and multiple scattering channel modeling [21], [22], [23], [24] for UV communications were studied using both analytical and stochastic methods. Recently, the impact of different weather conditions on the UV channels was theoretically studied in [25]. The channel capacities under on-off keying and pulse-position modulations for UV communications were numerically studied in [26], [27], and [28], where the inter-symbol-interference (ISI) was considered. The estimation of the channel ISI was studied in [29] and [30] and pilot bits were designed to improve estimation performance. The UV full-duplex techniques were studied in [31], [32], and [33], where the self-interference effect between the transmitting and receiving links was studied. Diversity reception techniques were adopted to enhance the NLOS links and mitigate the

¹Another promising technique is the Terahertz (THz) communication [13], [14], which also enjoys low background noise, good local security, and NLOS capability compared with traditional optical communications. However, the NLOS capability of UV signals comes from the scattering effects when UV signals reach microscopic particles in the atmosphere; while the NLOS capability of THz signals is mainly due to the reflecting effects when THz signals reach macroscopic obstacles, though the reflecting effect here is also attributed to the scattering effect of large amount of particles contained in the obstacles [15]. Therefore, it is challenging for THz signals to achieve NLOS communication in the atmosphere without reflection of macroscopic obstacles.

impact of turbulence on UV communications in [34], [35], and [36]. Besides, experimental studies on the NLOS UV communications were also performed by using both UV light-emitting diode (LED) and laser sources [37], [38], [39], [40]. However, so far only limited works focused on the NLOS UV positioning techniques.

There are at least two major benefits of studying NLOS UV positioning techniques. First, the NLOS UV positioning can be used to improve the NLOS link performance of UV communications. It was demonstrated that the receiving signal power in NLOS UV communications mainly comes from the single-scattering effect [17], [18], [19], [20] in short-range communication systems. The single-scattering link can be established only if the transmitting beam and the receiving field-of-view (FOV) share a common volume in the atmosphere. Therefore, if the receiver can obtain the location and pointing information of the transmitter, it can maintain the single-scattering link even in mobile scenarios. Second, the NLOS UV positioning is necessary for initializing the ad-hoc or mesh UV networks [9], [10], [11]. For example, in an ad-hoc UV network, each node has to search for its neighbor nodes first and then establish the NLOS links between the neighbor nodes and itself. Therefore, NLOS UV positioning can find its position in both civil and military communication networks. For example, the NLOS UV positioning combined with the NLOS UV communication can be deployed in either automation factories and medical equipment factories under electromagnetic sensitive environments, or in small battlefields under electromagnetic shielding scenarios.

B. Related Works

The optical positioning using visible lights has been elaborately studied in the existing literatures. Due to the high requirement for precise synchronization or narrow light pulses, time-of-arrive (TOA) [41] or time-difference-of-arrival (TDOA) [42] based visible light positioning (VLP) systems have rarely been realized in practice [43]. Therefore, the received-signal-strength (RSS) [44], [45], [46] and angle-of-arrival (AOA) [43], [47] based VLP systems are most commonly studied in real implementations due to their advantages of low-cost and centimeter-level accuracy. In the RSS based VLP systems, the Lambertian model is widely used to estimate the location from the RSS. However, Lambertian model does not well math the practical illumination pattern of available LED products. Though fingerprints or artificial neural networks can be employed to enhance the positioning performance of RSS based VLP systems, they require powerful signal processing units. The AOA based VLP is considered as the most promising scheme in VLP systems [43]. However, AOA based VLP systems are sensitive to the receivers' tilting angles. To tackle this issue, the angle-difference-of-arrival (ADOA) [48] based VLP was proposed, where the position is estimated by the ADOA of the LED signals. Since the ADOA values are irrelevant to the receiver rotation, the ADOA based VLP is immune to the receiving tilting. However, the ADOA algorithm is quadratic with the number of LEDs, which suffers from high time complexity. Besides, due to the requirement of

line-of-sight links between the LEDs and the receivers, all the VLP systems mentioned above can fail in the scenarios where only NLOS links are available. Since UV signals can achieve NLOS links due to its strong scattering effects when travelling in the atmosphere, we focus on the NLOS UV positioning in this work.

There are only limited works relating to the NLOS UV positioning. For example, early works [49], [50] are simple variants of traditional triangulation positioning method adopted in RF positioning techniques. However, these works [49], [50] assumed that the receivers know the exact transmitting elevation angle. Other related works were proposed as neighbor discovery protocols in ad-hoc UV networks [51], [52], [53]. For example, two neighbor discovery protocols with and without direction synchronization were proposed in [51], which were improved in [52] to alleviate effects of collisions. Besides, a faster discovery protocol was proposed by introducing a more efficient feedback mechanism in [53]. However, all these works [51], [52], [53] require each node be placed vertically. Besides, they can only obtain rough directions instead of the positions of neighbor nodes. A more precise method was proposed in [54], where the incoming angle of the transmitter can be estimated by two adjacent antennas in an omnidirectional antenna array with the same elevation angles. It was demonstrated that the estimation accuracy of the incoming angles can achieve 3° under typical system geometries [54]. However, the estimation method in [54] requires that the transmitter points to the receiver in advance and it cannot estimate the distance and the pointing angles of the transmitter. Therefore, NLOS UV positioning methods suitable for arbitrary transmitter pointing direction are still desirable.

C. Contributions

In a previous work [55], we proposed a NLOS UV positioning method by using two photon-counting receivers, where both the location and the pointing direction of the unknown transmitter can be estimated for arbitrary transmitter pointing direction. However, as we will demonstrate in the numerical results, two receivers can result in multiple-solution problems. Besides, the proposed NLOS UV positioning method in [55] cannot be applied to the scenarios where each node only has one receiver with fixing receiving elevation angle, which is usually the case in ad-hoc UV networks. For example, a transceiver in [51] with fixing elevation receiving angles was employed to standardize the nodes design and to facilitate the neighbor discovery process in a UV ad-hoc network. Therefore, it is necessary to extend our previous work to a more general scenario.

In this work, we focus on NLOS UV positioning techniques using photon-counting receivers, where N receivers are equidistantly arrayed in a line with a separate distance. There are three major differences between this work and our previous work in [55]. First, we extended the positioning method in [55] to multiple receivers to avoid the multiple solution problem. Second, we extended the positioning method in [55] to the case with separating receivers to account for the case where all the nodes are designed with fixing transmitting elevation angles.

Since the solving of distance and azimuth angle becomes coupled with each other, new positioning method is required. Third, we derived the Cramér-Rao bounds for estimating the distance and the azimuth angle when the separate distance equals zero, which can provide some insights on the performance limits of the proposed NLOS UV positioning method.

The key assumption in the proposed NLOS UV positioning method is based on the fact that the maximum receiving power of each receiver corresponds to the geometry case when its receiving axis intersects with the transmitting axis. We first derive both the geometrical and physical constraints for NLOS UV positioning techniques. Then we propose two NLOS UV positioning methods when $d_0 \neq 0$ and $d_0 = 0$, where d_0 is the separate distance between two adjacent receivers, as shown in Fig. 1(a). We further derive the Cramér-Rao bounds for estimating the location parameters when $d_0 = 0$. At last, we use Monte-Carlo simulation methods to explore the positioning performance of the proposed NLOS UV positioning methods using photon-counting receivers. The main contributions of this work are summarized as follows:

- We propose a NLOS UV positioning method using N linearly-arrayed photon-counting receivers with separate distance $d_0 \neq 0$, where both the location and the pointing direction of the transmitter can be estimated. We further consider the NLOS UV positioning method using N photon-counting receivers with separate distance $d_0 = 0$ and derived the Cramér-Rao bounds for estimating the location parameters.
- We demonstrate that the positioning error for $d_0 \neq 0$ using linearly-arrayed receivers will decrease first fast then slowly as the separate distance or the transmitting power increases. Besides, we demonstrate that the proposed NLOS UV positioning using N photon-counting receivers can achieve a positioning error less than 2 m when the transmitting elevation angle is greater than 30° and the separate distance is greater than 2 m.
- We demonstrate that at least three receivers are needed to avoid multiple-solution problem of the proposed NLOS UV positioning method. However, more than three receivers can only bring incremental gain to the positioning performance; and therefore, three receivers are enough for NLOS UV positioning method.
- We demonstrate that the proposed UV positioning methods with $d_0 \neq 0$ and $d_0 = 0$ have their respective advantages. The positioning method with $d_0 \neq 0$ can be used in cooperating positioning scenarios where each node has only one receiver with fixing receiving azimuth angle; whereas the positioning method with $d_0 = 0$ m can be used in independent positioning scenarios where each node can detect the UV signals at different receiving azimuth angles.

The rest of this paper is organized as follows. We first introduce the geometrical and physical constraints for UV positioning in Section II. Then we introduce two NLOS UV positioning methods for $d_0 \neq 0$ and $d_0 = 0$ in Section III. Then we present some numerical results on the positioning

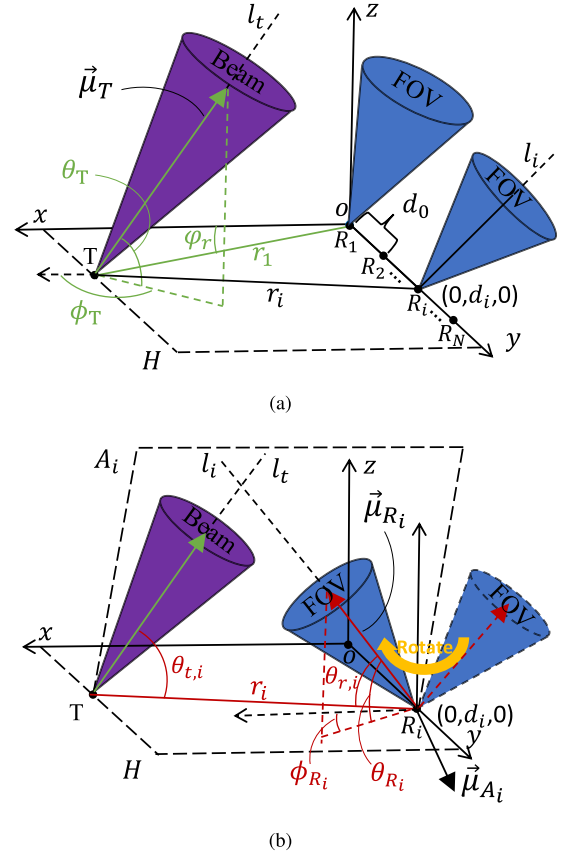


Fig. 1. System geometry of NLOS UV positioning: (a) transceiver geometry setting; (b) geometry for constraints.

performance of the proposed NLOS UV positioning method in Section IV. Finally, we conclude our work in Section V.

II. GEOMETRICAL AND PHYSICAL CONSTRAINTS FOR NLOS UV POSITIONING

The system geometry setting of the NLOS UV positioning using N linearly-arrayed receivers are shown in Fig. 1(a). The first receiver $R_1(0, 0, 0)$ locates at the origin of the $o(x-y-z)$ coordinate system and the i th receiver $R_i(0, d_i, 0)$ locates at the y -axis, where $i = 1, 2, \dots, N$ and $d_i = (i - 1)d_0$ is the distance between R_i and R_1 ; and d_0 is the separate distance between two adjacent receivers. An unknown transmitter $T(r_1 \cos \phi_r, r_1 \sin \phi_r, 0)$ locates at the $x - o - y$ plane H , where r_1 is the distance between the transmitter T and the receiver R_1 and ϕ_r is the azimuth angle between the vector $\vec{R_1T}$ and the x -axis. The central axes for the transmitting beam and the FOV of R_i are denoted by rays l_t and l_i , respectively. Without loss of generality, we assume that all the receivers have the same FOV angles and receiving areas. The distance between R_i and T is denoted by r_i . The direction of the transmitter can be represented by the direction cosine of ray l_t , i.e., $\vec{\mu}_T = [\cos \theta_T \cos \phi_T, \cos \theta_T \sin \phi_T, \sin \theta_T]^T$, where θ_T and ϕ_T are the transmitting elevation angle and the transmitting azimuth angle of ray l_t , respectively.

We consider two typical scenarios of NLOS UV positioning. The first is the positioning assisted NLOS UV communication scenario, where the NLOS positioning is employed to maintain the single-scattering links between the transceivers and can be

achieved by multiple receivers in the same node with $d_0 = 0$. The second is the neighbor discovery scenario in UV networks, where the NLOS positioning is employed to initializing the positioning of nodes in a mesh or ad-hoc UV network and can be achieved either by multiple nodes with $d_0 \neq 0$ or by single node with $d_0 = 0$.

Then the goal of the NLOS UV positioning is to obtain the location parameters $\{r_1, \phi_r\}$ and the pointing parameters $\{\theta_T, \phi_T\}$ of the transmitter. To achieve this, each receiver can rotate its FOV around its vertical axis with a pre-chosen elevation angle $\theta_{R_i} \in (0, \pi/2)$ and find the direction with the maximum receiving power (MRP) P_{R_i} and the corresponding receiving azimuth angle (RAA) ϕ_{R_i} , as shown in Fig. 1(b). The key assumption in our NLOS UV positioning method is based on the fact that the MRP P_{R_i} of the i th receiver corresponds to the geometry case that l_i intersect with l_t . In the following, we will present the geometrical constraints and physical constraints for the proposed NLOS UV positioning methods.

A. Geometrical Constraints

The direction cosines of rays l_i is denoted by $\vec{\mu}_{R_i}$ with $i \in \{1, 2, \dots, N\}$, which can be expressed as $\vec{\mu}_{R_i} = [\cos \theta_{R_i} \cos \phi_{R_i}, \cos \theta_{R_i} \sin \phi_{R_i}, \sin \theta_{R_i}]^T$. The plane formed by l_i and l_t is denoted by A_i . Then the normal vector $\vec{\mu}_{A_i}$ for planes A_i can be obtained as the cross product of $\vec{\mu}_{R_i}$ and $\overrightarrow{R_i T}$, i.e.,

$$\vec{\mu}_{A_i} = \vec{\mu}_{R_i} \times \overrightarrow{R_i T}, \quad (1)$$

where \times denotes the cross product operation and we have $\overrightarrow{R_i T} = [r_1 \cos \phi_r, r_1 \sin \phi_r - d_i, 0]^T$.

Because ray l_t locates at all the planes $\{A_1, A_2, \dots, A_N\}$, the vector $\vec{\mu}_T$ is perpendicular to all $\vec{\mu}_{A_i}$ for $i = 1, 2, \dots, N$. Using the fact $\vec{\mu}_T \cdot \vec{\mu}_{A_i} = 0$, where \cdot denotes the dot product operation, we can obtain the geometrical constraint for the i th receiver as

$$\begin{aligned} & \sin \theta_T [r_1 \sin(\phi_r - \phi_{R_i}) - d_i \cos \phi_{R_i}] \\ &= \cos \theta_T \tan \theta_{R_i} [r_1 \sin(\phi_r - \phi_T) - d_i \cos \phi_T]. \end{aligned} \quad (2)$$

B. Physical Constraints

Besides the N geometrical relations we have obtained above, the receiving powers in NLOS UV links are also closely related to the system geometry. We can establish N physical relations by using the channel path loss model of NLOS UV communications. The first channel model for ultraviolet communications was proposed by Luettgen in 1991 [17] in a coplanar geometry. After that, various channel models are proposed for both single-scattering [17], [18], [19], [20] and multiple scattering cases [21], [22], [23], [24].

When the transmitting beam divergence angle β_t and the receiving FOV angle β_r are given, the channel path loss depends only on the baseline distance r , the elevation angle θ_t of the transmitter, and the elevation angle of the receiver θ_r . Therefore, we can express the channel path loss as a function of r , θ_t , and θ_r , i.e., $L(r, \theta_t, \theta_r)$. If we consider the NLOS

link in plane A_i , we can obtain the elevation angle $\theta_{t,i}$ as a function of r_1 , ϕ_r , θ_T , and ϕ_T , i.e.,

$$\theta_{t,i}(r_1, \phi_r, \theta_T, \phi_T) = \arccos \left(\frac{\vec{\mu}_T \cdot \overrightarrow{T R_i}}{r_i} \right), \quad (3)$$

where r_i is the distance between the transmitter T and the i th receiver R_i ; and r_i can be expressed as a function of r_1 and ϕ_r , i.e.,

$$r_i(r_1, \phi_r) = \sqrt{r_1^2 + d_i^2 - 2d_i r_1 \sin \phi_r}. \quad (4)$$

Similarly, the elevation angle $\theta_{r,i}$ can be expressed as a function of r_1 and ϕ_r , i.e.,

$$\theta_{r,i}(r_1, \phi_r) = \arccos \left(\frac{\vec{\mu}_{R_i} \cdot \overrightarrow{R_i T}}{r_i} \right). \quad (5)$$

Then we can obtain a physical constraint by expressing the MRP P_{R_i} using the channel path loss model as

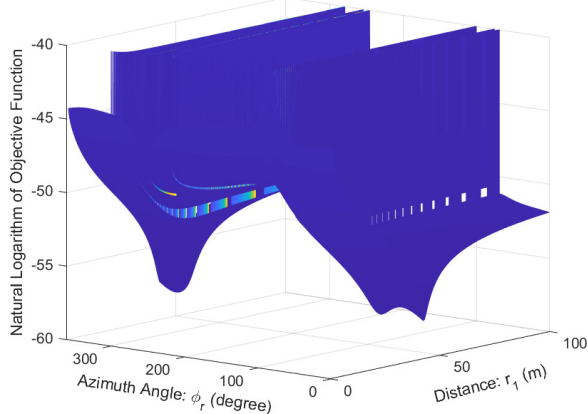
$$P_{R_i} = P_t L(r_i(r_1, \phi_r), \theta_{t,i}(r_1, \phi_r, \theta_T, \phi_T), \theta_{r,i}(r_1, \phi_r)), \quad (6)$$

where P_t is the transmitting power; $\theta_{t,i}(r_1, \phi_r, \theta_T, \phi_T)$, $r_i(r_1, \phi_r)$, and $\theta_{r,i}(r_1, \phi_r)$ are given in (3), (4), and (5), respectively.

By now, we have obtained $2N$ independent equations related to the location $\{r_1, \phi_r\}$ and the pointing $\{\theta_T, \phi_T\}$ of the transmitter T as follows:

$$\left\{ \begin{aligned} & \sin \theta_T [r_1 \sin(\phi_r - \phi_{R_1}) - d_1 \cos \phi_{R_1}] \\ &= \cos \theta_T \tan \theta_{R_1} [r_1 \sin(\phi_r - \phi_T) - d_1 \cos \phi_T] \\ & \cdots \\ & \sin \theta_T [r_1 \sin(\phi_r - \phi_{R_N}) - d_N \cos \phi_{R_N}] \\ &= \cos \theta_T \tan \theta_{R_N} [r_1 \sin(\phi_r - \phi_T) - d_N \cos \phi_T] \\ & P_{R_1} = P_t L(r_1(r_1, \phi_r), \theta_{t,1}(r_1, \phi_r, \theta_T, \phi_T), \theta_{r,1}(r_1, \phi_r)) \\ & \cdots \\ & P_{R_N} = P_t L(r_N(r_1, \phi_r), \theta_{t,N}(r_1, \phi_r, \theta_T, \phi_T), \theta_{r,N}(r_1, \phi_r)). \end{aligned} \right. \quad (7)$$

Let us inspect all the parameters in the simultaneous equations (7). The distance d_i , receiving elevation angle θ_{R_i} , RAA ϕ_{R_i} , MRP P_{R_i} , receiving area A_r , and FOV angle β_r in (7) are related to the receiver sides, which can be regarded as known parameters. Besides, when the transmitter and the receiver belong to two friendly users, e.g., in a UV communication network, the receiver side also knows the transmitting power P_t and the beam divergence angle β_t . By contrast, the receiver side usually has zero information on the elevation angle θ_T and the azimuth angle ϕ_T of the transmitter in practical implementations. Therefore, there are only four unknown parameters $\{r_1, \phi_r, \theta_T, \phi_T\}$ in the simultaneous equations (7). In the following section, we will provide two UV positioning methods using linearly-arrayed photon-counting receivers for solving $\{r_1, \phi_r, \theta_T, \phi_T\}$ for the cases of separate distance $d_0 \neq 0$ and $d_0 = 0$.

Fig. 2. Natural logarithm of the objective function under different r_1 and ϕ_r .

III. NLOS UV POSITIONING METHODS USING PHOTON-COUNTING RECEIVERS

A. NLOS UV Positioning Method When $d_0 \neq 0$

We consider a general case with $d_0 \neq 0$ first. Because the parameters $\{r_1, \phi_r, \theta_T, \phi_T\}$ to be estimated are coupled with each other in (7), it is challenging to analytically solve the simultaneous equations (7); and we have to adopt numerical searching methods. Solving (7) is equivalent to solve the following optimization problem:

$$\begin{aligned} & \{r_1^*, \phi_r^*, \theta_T^*, \phi_T^*\} \\ = & \underset{r_1, \phi_r, \theta_T, \phi_T}{\operatorname{argmin}} \sum_{i=1}^N F_i^2(r_1, \phi_r, \theta_T, \phi_T) \\ & + G_i^2(r_1, \phi_r, \theta_T, \phi_T) \\ \text{s.t. } & 0 < r_1 \leq r_{max} \\ & 0 \leq \phi_r < 2\pi \\ & 0 < \theta_T \leq \pi/2 \\ & 0 \leq \phi_T < 2\pi, \end{aligned} \quad (8)$$

where $F_i(r_1, \phi_r, \theta_T, \phi_T) \triangleq \sin \theta_T [r_1 \sin(\phi_r - \phi_{R_i}) - d_i \cos \phi_{R_i}] - \cos \theta_T \tan \theta_{R_i} [r_1 \sin(\phi_r - \phi_T) - d_i \cos \phi_T]$ and $G_i(r_1, \phi_r, \theta_T, \phi_T) \triangleq P_t L(r_i(r_1, \phi_r), \theta_{t,i}(r_1, \phi_r, \theta_T, \phi_T), \theta_{r,i}(r_1, \phi_r)) - P_{R_i}$ for $i \in \{1, 2, \dots, N\}$; r_{max} is the maximum searching range for r_1 .

It is challenging to prove the convexity of the objective function in (8). Fig. 2 present an example of the objective function under different r_1 and ϕ_r for given θ_T and ϕ_T . We can see that the objective function is far from a convex function. Therefore, ordinary gradient-based algorithms cannot be applied since they will be trapped in local optimum solutions. Therefore, we have to use the brute-force method for searching the optimal solution. When a brute-force search is adopted, the time complexity becomes $O\left(\frac{1}{\Delta r_1} \frac{1}{\Delta \phi_r} \frac{1}{\Delta \theta_T} \frac{1}{\Delta \phi_T}\right)$, where Δr_1 , $\Delta \phi_r$, $\Delta \theta_T$, and $\Delta \phi_T$ are the searching precisions for r_1 , ϕ_r , θ_T , and ϕ_T , respectively. For typical implementations in short ranges, we can set $r_{max} = 150$ m, $\Delta r_1 = 0.1$ m, and $\Delta \phi_r = \Delta \theta_T = \Delta \phi_T = 0.1^\circ$, then the time complexity can be estimated as $O(1.75 \times 10^{13})$, which is extremely time consuming and nearly impossible to be applied in practical

systems. In the following, we present an improved method with an acceptable time complexity.

1) Improved NLOS UV Positioning Method When $d_0 \neq 0$:

The four parameters $\{r_1, \phi_r, \theta_T, \phi_T\}$ are coupled with each other in (8). To simplify the optimization problem, we will first decouple the location parameters $\{r_1, \phi_r\}$ from the pointing parameters $\{\theta_T, \phi_T\}$, and then propose a more efficient positioning method for $d_0 \neq 0$.

From the first N equations in (7), we can observe that θ_T and ϕ_T can be uniquely determined once r and ϕ_r are given due to the geometrical constraints. Therefore, if we can express θ_T and ϕ_T as analytical forms of r and ϕ_r , then we can use the last N equations in (7) for searching the location parameters (r, ϕ_r) first and then obtain the pointing parameters $\{\theta_T, \phi_T\}$ accordingly. To achieve this, we will reform the first N equations by using the Cartesian coordinate system.

The location of the transmitter T can be equivalently represented by its Cartesian coordinates $T(T_x, T_y, 0)$ with $T_x = r_1 \cos \phi_r$ and $T_y = r_1 \sin \phi_r$. Then we can rewrite $\vec{\mu}_{A_i}$ as

$$\vec{\mu}_{A_i} = \begin{bmatrix} (d_i - T_y) \sin \theta_{R_i} \\ T_x \sin \theta_{R_i} \\ ((T_y - d_i) \cos \phi_{R_i} - T_x \sin \phi_{R_i}) \cos \theta_{R_i} \end{bmatrix}. \quad (9)$$

Similarly, the direction vector of l_t can be represented by its Cartesian coordinates $\vec{l}_t = [l_{t,x}, l_{t,y}, l_{t,z}]^T$. Without loss of generality, we can choose $l_{t,z} = 1$ such that

$$\begin{cases} l_{t,x} = \cot \theta_T \cos \phi_T \\ l_{t,y} = \cot \theta_T \sin \phi_T. \end{cases} \quad (10)$$

Then by using the relation $\vec{l}_t \cdot \vec{\mu}_{A_i} = 0$, we can rewrite the first N equations in (7) as

$$\begin{cases} l_{t,x} \mu_{A_1,x} + l_{t,y} \mu_{A_1,y} = -\mu_{A_1,z} \\ l_{t,x} \mu_{A_2,x} + l_{t,y} \mu_{A_2,y} = -\mu_{A_2,z} \\ \dots \\ l_{t,x} \mu_{A_N,x} + l_{t,y} \mu_{A_N,y} = -\mu_{A_N,z}, \end{cases} \quad (11)$$

where $\mu_{A_i,x} \triangleq (d_i - T_y) \sin \theta_{R_i}$, $\mu_{A_i,y} \triangleq T_x \sin \theta_{R_i}$, and $\mu_{A_i,z} \triangleq ((T_y - d_i) \cos \phi_{R_i} - T_x \sin \phi_{R_i}) \cos \theta_{R_i}$ for $i \in \{1, 2, \dots, N\}$. Now the first N geometrical constraints can be rewritten as linear equations $\mathbf{X}l = \mathbf{y}$, where $l \triangleq [l_{t,x}, l_{t,y}]^T$, $\mathbf{y} \triangleq [-\mu_{A_1,z}, -\mu_{A_2,z}, \dots, -\mu_{A_N,z}]^T$, and \mathbf{X} is defined as

$$\mathbf{X} \triangleq \begin{bmatrix} \mu_{A_1,x} & \mu_{A_1,y} \\ \mu_{A_2,x} & \mu_{A_2,y} \\ \dots & \dots \\ \mu_{A_N,x} & \mu_{A_N,y} \end{bmatrix}. \quad (12)$$

Then the parameters l can be solved by using the least square method as [56]

$$l = (\mathbf{X}^T \mathbf{X})^{-1} \mathbf{X}^T \mathbf{y}. \quad (13)$$

After some algebra, we can further obtain $l_{t,x}$ and $l_{t,y}$ as eq. (14), shown at the bottom of the next page, (see Appendix A).

Then according to (10), we can obtain the elevation angle θ_T and the azimuth angle ϕ_T as a function of r_1 and ϕ_r , i.e.,

$$\begin{cases} \theta_T(r_1, \phi_r) = \arctan\left(\sqrt{\frac{1}{l_{t,x}^2(r_1, \phi_r) + l_{t,y}^2(r_1, \phi_r)}}\right) \\ \phi_T(r_1, \phi_r) = \arctan\left(\frac{l_{t,y}(r_1, \phi_r)}{l_{t,x}(r_1, \phi_r)}\right) + k\pi, \end{cases} \quad (15)$$

where $k \in \mathbb{Z}$. When ϕ_T is restricted in $[0, 2\pi]$, there are two azimuth angles $\phi_{T,1}$ and $\phi_{T,2}$ satisfying (15), which are at inverse directions because $|\phi_{T,1} - \phi_{T,2}| = \pi$. Nevertheless, we can always choose the one with smaller $|\vec{\mu}_T \cdot \vec{\mu}_{A_1}|$.

In this context, the optimization problem in (8) is equivalent to the following two-dimensional optimization problem:

$$\begin{aligned} \{r_1^*, \phi_r^*\} = \operatorname{argmin}_{r_1, \phi_r} & \sum_{i=1}^N G_i^2(r_1, \phi_r, \theta_T(r_1, \phi_r), \phi_T(r_1, \phi_r)) \\ \text{s.t. } & 0 < r_1 \leq r_{max} \\ & 0 \leq \phi_r < 2\pi. \end{aligned} \quad (16)$$

Then the time complexity of solving (16) by using a brute-force search can be obtained as $O\left(\frac{1}{\Delta r_1} \frac{1}{\Delta \phi_r}\right)$. For typical implementations in short ranges with $r_{max} = 150$ m, $\Delta r_1 = 0.1$ m, and $\Delta \phi_r = 0.1^\circ$, the time complexity can be estimated as $O(5.4 \times 10^6)$, which is an acceptable time complexity in practical systems.

Besides, the calculating of the channel path loss $L(r, \theta_t, \theta_r)$ can be time consuming for multiple scattering channels in practical implementations. Because we use the brute-force searching method here, the effectiveness of the proposed NLOS UV positioning does not depend on the adopted channel model and different channel model will only affect the calculating speed for the channel path loss. Therefore, for simplicity, we can adopt an analytical single-scattering channel model proposed for small common volumes in [57], i.e.,

$$\begin{aligned} L(r, \theta_t, \theta_r) &= \frac{A_r k_s \beta_t^2 \beta_r p(\cos \theta_s) \sin \theta_s (12 \sin^2 \theta_r + \beta_r^2 \sin^2 \theta_t)}{96 r \sin \theta_t \sin^2 \theta_r (1 - \cos(\beta_t/2))} \\ &\times \exp\left(-\frac{k_e r (\sin \theta_t + \sin \theta_r)}{\sin \theta_s}\right), \end{aligned} \quad (17)$$

where A_r is the receiving area; $k_s = k_s^{Ray} + k_s^{Mie}$ is the scattering coefficient; k_s^{Ray} and k_s^{Mie} are the Rayleigh scattering coefficient and the Mie scattering coefficient, respectively; $k_e = k_a + k_s$ is the extinction coefficient and k_a is the absorption coefficient; $\theta_s = \theta_t + \theta_r$ is the scattering angle; $p(\cos \theta_s)$ is the scattering phase function, which can be obtained as a linear combining of the Rayleigh scattering function

$p^{Ray}(\cos \theta_s)$ and the Mie scattering function $p^{Mie}(\cos \theta_s)$, i.e., $p(\cos \theta_s) = \frac{k_s^{Ray}}{k_s} p^{Ray}(\cos \theta_s) + \frac{k_s^{Mie}}{k_s} p^{Mie}(\cos \theta_s)$, where the Rayleigh scattering function and the Mie scattering function are given by $p^{Ray}(\cos \theta_s) = \frac{3[1+3\gamma+(1-\gamma)\cos^2\theta_s]}{16\pi(1+2\gamma)}$ and $p^{Mie}(\cos \theta_s) = \frac{1-g^2}{4\pi} \left[\frac{1}{(1+g^2-2g\cos\theta_s)^{3/2}} + f \frac{0.5(3\cos^2\theta_s-1)}{(1+g^2)^{3/2}} \right]$, respectively, and where γ , f , and g are model parameters.

After obtaining the position (r_1^*, ϕ_r^*) , we can further obtain the pointing angles (θ_T^*, ϕ_T^*) of the transmitter according to (26).

2) *Special Case When $\theta_T = 90^\circ$* : An interesting case is that when $\theta_T = \pi/2$ is adopted in the whole UV network, which is the same case with References [51], [52], and [53]. In this case, the geometrical constraint at R_1 degenerates to $\sin(\phi_r - \phi_{R_1}) = 0$, which means $\phi_r = \phi_{R_1}$.

Besides, the geometrical constraints at $\{R_2, R_3, \dots, R_N\}$ becomes

$$\begin{cases} r_1 \sin(\phi_{R_1} - \phi_{R_2}) = d_2 \cos \phi_{R_2} \\ r_1 \sin(\phi_{R_1} - \phi_{R_3}) = d_3 \cos \phi_{R_3} \\ \dots \\ r_1 \sin(\phi_{R_1} - \phi_{R_N}) = d_N \cos \phi_{R_N}. \end{cases} \quad (18)$$

Then as long as $d_0 \neq 0$, we can obtain the distance r_1 by using the least square method as (see Appendix. A)

$$r_1 = \frac{\sum_{i=2}^N d_i \cos \phi_{R_i} \sin(\phi_{R_1} - \phi_{R_i})}{\sum_{i=2}^N \sin^2(\phi_{R_1} - \phi_{R_i})}. \quad (19)$$

We can see that in this case the location (r_1, ϕ_r) of the transmitter T can be simply determined by the geometrical constraints as long as $d_0 \neq 0$ when $\theta_T = \pi/2$, i.e., no physical constraint is needed.

B. NLOS UV Positioning Method When $d_0 = 0$

In above Section III-A, we have considered a general case with $d_0 \neq 0$, where the unknown parameters r_1 and ϕ_r are coupled with each other. In this section, we consider a generated case with $d_0 = 0$. There are two main reasons why considering this special case with $d_0 = 0$ is important. First, as long as each receiver can take multiple different receiving elevation angles, it is more convenient to implement the NLOS positioning with $d_0 = 0$ since we do not need to move the receiver during the positioning. Second, as we will demonstrate later, the unknown location parameters r_1 and ϕ_r will be further decoupled when $d_0 = 0$. Then we can perform some theoretical analysis on Cramér-Rao bounds of the positioning method.

When $d_0 = 0$, the NLOS UV positioning can be achieved at one single node. In this context, we have $R_1 = R_2 =$

$$\begin{cases} l_{t,x}(r_1, \phi_r) = \frac{-\left(\sum_{i=1}^N \mu_{A_i,y}^2\right) \left(\sum_{i=1}^N \mu_{A_i,x} \mu_{A_i,z}\right) + \left(\sum_{i=1}^N \mu_{A_i,x} \mu_{A_i,y}\right) \left(\sum_{i=1}^N \mu_{A_i,y} \mu_{A_i,z}\right)}{\left(\sum_{i=1}^N \mu_{A_i,x}^2\right) \left(\sum_{i=1}^N \mu_{A_i,y}^2\right) - \left(\sum_{i=1}^N \mu_{A_i,x} \mu_{A_i,y}\right)^2} \\ l_{t,y}(r_1, \phi_r) = \frac{\left(\sum_{i=1}^N \mu_{A_i,x} \mu_{A_i,y}\right) \left(\sum_{i=1}^N \mu_{A_i,x} \mu_{A_i,z}\right) - \left(\sum_{i=1}^N \mu_{A_i,x}^2\right) \left(\sum_{i=1}^N \mu_{A_i,y} \mu_{A_i,z}\right)}{\left(\sum_{i=1}^N \mu_{A_i,x}^2\right) \left(\sum_{i=1}^N \mu_{A_i,y}^2\right) - \left(\sum_{i=1}^N \mu_{A_i,x} \mu_{A_i,y}\right)^2}. \end{cases} \quad (14)$$

$\cdots = R_N \triangleq R(0, 0, 0)$ and $A_1 = A_2 = \cdots = A_N \triangleq A$; and therefore, we have $r_1 = r_2 = \cdots = r_N \triangleq r$ and $\theta_{t,1} = \theta_{t,2} = \cdots = \theta_{t,N} \triangleq \theta_t$.

By letting $d_0 = 0$ in (2), we can obtain the following N geometrical constrains:

$$\begin{cases} \tan \theta_T \sin(\phi_r - \phi_{R_1}) = \tan \theta_{R_1} \sin(\phi_r - \phi_T) \\ \cdots \\ \tan \theta_T \sin(\phi_r - \phi_{R_N}) = \tan \theta_{R_N} \sin(\phi_r - \phi_T). \end{cases} \quad (20)$$

From (20) we can see that the azimuth angle ϕ_r can be determined by the geometry constrains only, which is irrelevant to the distance r . Once ϕ_r is obtained, the distance r can be determined in plane A using the following N physical constrains:

$$\begin{cases} P_t L(r_1, \theta_t, \theta_{r,1}) = P_{R_1} \\ \cdots \\ P_t L(r_1, \theta_t, \theta_{r,N}) = P_{R_N}, \end{cases} \quad (21)$$

where $\theta_{r,i}$ for $i = 1, 2, \dots, N$ is the receiving elevation angle in plane A given by $\theta_{r,i} = \arccos(\cos \theta_{R_i} \cos(\phi_r - \phi_{R_i}))$.

In this context, the solving of ϕ_r and r can be decoupled into two separate steps: first we obtain ϕ_r by from (20), then we obtain r from (21).

1) *Obtaining ϕ_r :* Solving (20) is equivalent to finding a plane A determined by all receiving vectors $\{\vec{\mu}_{R_1}, \vec{\mu}_{R_2}, \dots, \vec{\mu}_{R_N}\}$. To achieve this, we first denote the normal vector of plane A by $\vec{\mu}_A \triangleq [\mu_{A,x}, \mu_{A,y}, \mu_{A,z}]^T$. Because the plane A must pass through the origin $(0, 0, 0)$, we can write the equation of A as $\mu_{A,x}x + \mu_{A,y}y + \mu_{A,z}z = 0$. Here we let the plane A be the one that minimizes the summation of the distances between the points $\{\vec{\mu}_{R_1}, \vec{\mu}_{R_2}, \dots, \vec{\mu}_{R_N}\}$ and the plane A , i.e.,

$$\begin{aligned} & \{\mu_{A,x}^*, \mu_{A,y}^*, \mu_{A,z}^*\} \\ &= \arg \min_{\mu_{A,x}, \mu_{A,y}, \mu_{A,z}} \sum_{i=1}^N (\mu_{A,x} \cos \theta_{R_i} \cos \phi_{R_i} \\ & \quad + \mu_{A,y} \cos \theta_{R_i} \sin \phi_{R_i} + \mu_{A,z} \sin \theta_{R_i})^2 \\ & \text{s.t. } \mu_{A,x}^2 + \mu_{A,y}^2 + \mu_{A,z}^2 = 1. \end{aligned} \quad (22)$$

To facilitate our analysis, we can rewrite $[\mu_{A,x}, \mu_{A,y}, \mu_{A,z}]^T$ in polar coordinates as $\mu_{A,x} = \cos \theta \cos \phi$, $\mu_{A,y} = \cos \theta \sin \phi$, and $\mu_{A,z} = \sin \theta$. We further define $a_i \triangleq \cos \theta_{R_i} \cos \phi_{R_i}$, $b_i \triangleq \cos \theta_{R_i} \sin \phi_{R_i}$, and $c_i \triangleq \sin \theta_{R_i}$. Then we can rewrite the optimization problem in (22) as

$$\begin{aligned} & \{\theta^*, \phi^*\} \\ &= \arg \min_{\theta, \phi} \sum_{i=1}^N (a_i \cos \theta \cos \phi + b_i \cos \theta \sin \phi + c_i \sin \theta)^2 \\ & \text{s.t. } -\pi/2 \leq \theta \leq \pi/2 \\ & \quad 0 \leq \phi < 2\pi. \end{aligned} \quad (23)$$

The optimization problem (23) can be solved by brute-force searching method with time complexity $O(\frac{1}{\Delta\theta\Delta\phi})$, where $\Delta\theta$ and $\Delta\phi$ are the searching precisions for θ and ϕ , respectively. For typical implementations with $\Delta\theta = \Delta\phi = 0.1^\circ$, the time complexity can be estimated as $O(6.48 \times 10^6)$, which is an acceptable time complexity in practical systems.

After obtaining the optimum θ^* and ϕ^* , the vector \overrightarrow{RT} can be directly obtained by intersecting plane A with the horizontal plane $H : z = 0$. Then the equation of line \overrightarrow{RT} can be easily obtained as $y = -\mu_{A,x}/\mu_{A,y}x = \tan \phi_r x$. Therefore, the optimal azimuth angle ϕ_r^* can be obtained as

$$\phi_r^* = \arctan\left(-\frac{\mu_{A,x}}{\mu_{A,y}}\right) + k\pi = \phi^* + (k - \frac{1}{2})\pi, \quad (24)$$

where $k \in \mathbb{Z}$. When ϕ_r is restricted in $[0, 2\pi]$, there are two azimuth angle $\phi_{r,1}$ and $\phi_{r,2}$ satisfying (24), which are at inverse directions because $|\phi_{r,1} - \phi_{r,2}| = \pi$. Nevertheless, we choose the one with larger receiving power, which corresponds to the one with $\vec{\mu}_{R_1} \cdot \overrightarrow{RT} > 0$.

2) *Obtaining r :* Solving (21) is equivalent to solving the following optimization problem:

$$\begin{aligned} \{r^*, \theta_t^*\} &= \operatorname{argmin}_{r, \theta_t} \sum_{i=1}^N [P_t L(r, \theta_t, \theta_{r,i}) - P_{R_i}]^2 \\ & \text{s.t. } 0 < r \leq r_{max} \\ & \quad 0 \leq \theta_t < \pi. \end{aligned} \quad (25)$$

Then the time complexity of solving (25) by using a brute-force search can be obtained as $O\left(\frac{1}{\Delta r_1} \frac{1}{\Delta \theta_t}\right)$. For typical implementations in short ranges with $r_{max} = 150$ m, $\Delta r_1 = 0.1$ m, and $\Delta \theta_t = 0.1^\circ$, the time complexity can be estimated as $O(2.7 \times 10^6)$, which is an acceptable time complexity in practical systems.

After obtaining θ_t^* , we can further obtain the pointing angles $\{\theta_T^*, \phi_T^*\}$ of the transmitter as

$$\begin{cases} \theta_T^* = \arcsin(|\sin \theta_t^* \cos \theta^*|) \\ \phi_T^* = \phi_r^* + \arccos\left(\frac{\cos \theta_t^*}{\cos \theta_T^*}\right) + k\pi, \end{cases} \quad (26)$$

where $k \in \mathbb{Z}$. When ϕ_T is restricted in $[0, 2\pi]$, there are two azimuth angle $\phi_{T,1}$ and $\phi_{T,2}$ satisfying (26) with $|\phi_{T,1} - \phi_{T,2}| = \pi$. Nevertheless, we choose the one with smaller $|\vec{\mu}_T \cdot \vec{\mu}_A|$.

We remark that when $d_0 = 0$, to obtain plane A , we must have $\theta_{R_i} \neq \theta_{R_j}$ when $i \neq j$. Therefore, the NLOS UV positioning method with $d_0 = 0$ cannot be applied to the scenarios where each node has only one receiver with fixing receiving azimuth angle.

C. Cramér-Rao Bounds When $d_0 = 0$

1) *Cramér-Rao Bound for Estimating ϕ_r :* The azimuth angle ϕ_r is obtained by measuring the RAAs. To derive the Cramér-Rao bound, we have to know the probability density functions (PDFs) of RAAs. In practical implementations, the measuring error of $\hat{\phi}_{R_i}$ can be mainly divided into two parts. The first part comes from the potential off-axis angle between the transmitting beam axis and the receiving FOV axis when the MRP is obtained. Because the receiver has zero prior information on the transmitting geometries, it is reasonable to assume that the measuring error due to the off-axis angle follows a zero-mean Gaussian distribution. The second part comes from the measuring error due to the employed instruments, e.g., a protractor or a goniometer; without loss of

generality, we can also assume that the measuring error due to employed instruments follows a zero-mean Gaussian distribution. Therefore, the estimated $\hat{\phi}_{R_i}$ approximately follows as a Gaussian distribution with mean ϕ_{R_i} and variance $\sigma_{\phi_{R_i}}^2$, i.e., [55]

$$f(\hat{\phi}_{R_i}) = \frac{\exp\left(-\frac{(\hat{\phi}_{R_i} - \phi_{R_i})^2}{2\sigma_{\phi_{R_i}}^2}\right)}{\sqrt{2\pi\sigma_{\phi_{R_i}}^2}}, \quad (27)$$

where the variance $\sigma_{\phi_{R_i}}^2$ is determined by the measuring process; and without loss of generality, we set $\sigma_{\phi_{R_1}}^2 = \sigma_{\phi_{R_2}}^2 = \dots = \sigma_{\phi_{R_N}}^2 \triangleq \sigma_{\phi_R}^2$. The mean value ϕ_{R_i} can be obtained by using the relation $\vec{\mu}_{R_i} \cdot (\vec{\mu}_T \times \vec{TR_i}) = 0$ as

$$\begin{aligned} \phi_{R_i} = & (-1)^k \arcsin \left(\frac{\tan \theta_{R_i} (r_1 \sin(\phi_T - \phi_r) + d_i \cos \phi_T)}{\tan \theta_T \sqrt{r_1^2 + d_i^2 - 2d_i r_1 \sin \phi_r}} \right) \\ & + \arctan \left(\frac{r_1 \sin \phi_r - d_i}{r_1 \cos \phi_r} \right) + k\pi, \end{aligned} \quad (28)$$

where $k \in \mathbb{Z}$. When ϕ_{R_i} is restricted in $[0, 2\pi]$, there are two azimuth angle $\phi_{R,i}^1$ and $\phi_{R,i}^2$ satisfying (28). Nevertheless, we choose the one with larger receiving power, which corresponds to the one with $\vec{\mu}_{R_i} \cdot \vec{R_i T} > 0$.

Then for N receivers, the joint PDF of all RAAs can be expressed as a joint Gaussian PDF as

$$f(\hat{\phi}_{R_1}, \hat{\phi}_{R_2}, \dots, \hat{\phi}_{R_N}) = \frac{\exp\left(-\sum_{i=1}^N \frac{(\hat{\phi}_{R_i} - \phi_{R_i})^2}{2\sigma_{\phi_R}^2}\right)}{(2\pi)^{N/2} \prod_{i=1}^N \sigma_{\phi_R}}, \quad (29)$$

where the theoretical RAA ϕ_{R_i} can be obtained by substituting $d_i = 0$ into (28), i.e.,

$$\phi_{R_i} = \phi_r + \arcsin \left(\frac{\tan \theta_{R_i} \sin(\phi_T - \phi_r)}{\tan \theta_T} \right), \quad (30)$$

and where we have chosen $k = 0$ without loss of generality.

Then the log-likelihood function of an observation $\{\hat{\phi}_{R_1}, \hat{\phi}_{R_2}, \dots, \hat{\phi}_{R_N}\}$ conditioned on a given parameter ϕ_r is defined as $L_{\phi_r} \triangleq \ln f(\hat{\phi}_1, \hat{\phi}_2, \dots, \hat{\phi}_N; \phi_r)$, which can be obtained as

$$L_{\phi_r} = -\ln \left((2\pi)^{N/2} \prod_{i=1}^N \sigma_{\phi_R} \right) - \sum_{i=1}^N \frac{(\hat{\phi}_{R_i} - \phi_{R_i})^2}{2\sigma_{\phi_R}^2}. \quad (31)$$

Then we can obtain the two order derivative $\frac{\partial^2 L_{\phi_r}}{\partial \phi_r^2}$ as

$$\frac{\partial^2 L_{\phi_r}}{\partial \phi_r^2} = \sum_{i=1}^N \frac{1}{\sigma_{\phi_R}^2} \left[(\hat{\phi}_{R_i} - \phi_{R_i}) \frac{\partial^2 \phi_{R_i}}{\partial \phi_r^2} - \left(\frac{\partial \phi_{R_i}}{\partial \phi_r} \right)^2 \right]. \quad (32)$$

Then the Fisher information of parameter ϕ_r can be obtained as [58]

$$I_{\phi_r} \triangleq E \left[-\frac{\partial^2 L_{\phi_r}}{\partial \phi_r^2} \right] = \sum_{i=1}^N \frac{1}{\sigma_{\phi_R}^2} \left(\frac{\partial \phi_{R_i}}{\partial \phi_r} \right)^2, \quad (33)$$

where we have used the equality $E[\hat{\phi}_{R_i} - \phi_{R_i}] = 0$, and here $\frac{\partial \phi_{R_i}}{\partial \phi_r}$ can be obtained as

$$\frac{\partial \phi_{R_i}}{\partial \phi_r} = 1 - \frac{\tan \theta_{R_i} \cos(\phi_T - \phi_r)}{\sqrt{\tan^2 \theta_T - \tan^2 \theta_{R_i} \sin^2(\phi_T - \phi_r)}}. \quad (34)$$

When the fluctuation of $\hat{\phi}_{R_i}$ is small, $\hat{\phi}_r$ can be regarded as an unbiased estimate of ϕ_r . Then the Cramér-Rao bound [58] for the estimating ϕ_r can be obtained as

$$\text{Var}[\phi_r] \geq \frac{1}{I_{\phi_r}} = \frac{\sigma_{\phi_R}^2}{\sum_{i=1}^N \left(\frac{\partial \phi_{R_i}}{\partial \phi_r} \right)^2}. \quad (35)$$

From (35), we can observe that the Cramér-Rao bound for the estimating ϕ_r will decrease as the number of receivers increases or the measuring error $\sigma_{\phi_R}^2$ decreases.

2) *Cramér-Rao Bound for Estimating r* : The distance r is obtained by measuring the MRPs. Therefore, we have to know the PDFs of MRPs. When photon-counting receivers are adopted to measure the MRP for a given receiving azimuth angle ϕ_{R_i} , we can measure the output number of photons n_i in a measuring duration T_d and estimate the MRP as

$$\hat{P}_{R_i} = \frac{n_i h \nu}{T_d}, \quad (36)$$

where h is the plank constant; $\nu = c/\lambda$ is the frequency of the transmitted UV light; c is the light speed and λ is the wavelength of UV light. For a given light intensity, the output of the photon-counting receiver satisfies a Poisson distribution with probability density given by [26], [27], and [28]

$$p(n_i) = \frac{(\lambda_i)^{n_i} \exp(-\lambda_i)}{n_i!}, \quad (37)$$

where $\lambda_i = \frac{P_t L(r, \theta_t, \theta_{r,i}) T_d}{h \nu}$ is the average receiving number of photons at the azimuth angle ϕ_{R_i} of the i th photon-counting receiver. Then the probability density of the MRP can be expressed as

$$p(\hat{P}_{R_i}) = \frac{T_d}{h \nu} \frac{(\lambda_i)^{\frac{\hat{P}_{R_i} T_d}{h \nu}} \exp(-\lambda_i)}{\left(\frac{\hat{P}_{R_i} T_d}{h \nu} \right)!}, \quad (38)$$

where $\hat{P}_{R_i} \in \{0, \frac{h \nu}{T_d}, 2 \frac{h \nu}{T_d}, 3 \frac{h \nu}{T_d}, \dots\}$.

It is challenging to derive the Cramér-Rao bound from the probability density given in (38). For simplicity, we can approximate $\hat{P}_{R,i}$ as a Gaussian distribution when λ_i is large due to the fact that Poisson distribution can be approximated as Gaussian distribution when the strength is large. Then the joint PDF of all MRPs can be approximated as a joint Gaussian PDF, i.e.,

$$f(\hat{P}_{R_1}, \hat{P}_{R_2}, \dots, \hat{P}_{R_N}) \approx \frac{\exp\left(-\sum_{i=1}^N \frac{(\hat{P}_{R_i} - P_{R_i})^2}{2\sigma_{P_{R_i}}^2}\right)}{(2\pi)^{N/2} \prod_{i=1}^N \sigma_{P_{R_i}}}, \quad (39)$$

where both the mean values P_{R_i} and the variances $\sigma_{P_{R_i}}^2$ are related to the distance r ; and we can obtain P_{R_i} and $\sigma_{P_{R_i}}^2$ as

$$\begin{cases} P_{R_i} = P_t L(r, \theta_t, \theta_{r,i}) \\ \sigma_{P_{R_i}}^2 = \frac{P_t L(r, \theta_t, \theta_{r,i}) h \nu}{T_d}, \end{cases} \quad (40)$$

where $L(r, \theta_t, \theta_{r,i})$ can be obtained from (17) without loss of generality.

Then the log-likelihood function of an observation $\{\hat{P}_{R_1}, \hat{P}_{R_2}, \dots, \hat{P}_{R_N}\}$ conditioned on a given parameter r can be obtained as $L_r \triangleq \ln f(\hat{P}_{R_1}, \hat{P}_{R_2}, \dots, \hat{P}_{R_N}; r)$, which can be obtained as

$$L_r = -\ln \left((2\pi)^{N/2} \prod_{i=1}^N \sigma_{P_{R_i}} \right) - \sum_{i=1}^N \frac{(\hat{P}_{R_i} - P_{R_i})^2}{2\sigma_{P_{R_i}}^2}. \quad (41)$$

If we omit the impact of $\hat{\phi}_r$ on estimating r , then the two order derivative $\frac{\partial^2 L_r}{\partial r^2}$ can be obtained as

$$\begin{aligned} \frac{\partial^2 L_r}{\partial r^2} = & -\sum_{i=1}^N \frac{1}{\sigma_{P_{R_i}}^2} \left[\frac{1}{2} \left(1 - \frac{(\hat{P}_{R_i} - P_{R_i})^2}{\sigma_{P_{R_i}}^2} \right) \frac{\partial^2 \sigma_{P_{R_i}}^2}{\partial r^2} \right. \\ & - (\hat{P}_{R_i} - P_{R_i}) \frac{\partial^2 P_{R_i}}{\partial r^2} + \left(\frac{\partial P_{R_i}}{\partial r} \right)^2 \\ & + \left(\frac{(\hat{P}_{R_i} - P_{R_i})^2}{\sigma_{P_{R_i}}^4} - \frac{1}{2\sigma_{P_{R_i}}^2} \right) \left(\frac{\partial \sigma_{P_{R_i}}^2}{\partial r} \right)^2 \\ & \left. + 2 \frac{\hat{P}_{R_i} - P_{R_i}}{\sigma_{P_{R_i}}^2} \frac{\partial \sigma_{P_{R_i}}^2}{\partial r} \frac{\partial P_{R_i}}{\partial r} \right]. \end{aligned} \quad (42)$$

Using the relations $E[\hat{P}_{R_i} - P_{R_i}] = 0$ and $E[(\hat{P}_{R_i} - P_{R_i})^2] = \sigma_{P_{R_i}}^2$, we can obtain the Fisher information for estimating r as

$$I_r = \sum_{i=1}^N \frac{1}{\sigma_{P_{R_i}}^2} \left[\left(\frac{\partial P_{R_i}}{\partial r} \right)^2 + \frac{1}{2\sigma_{P_{R_i}}^2} \left(\frac{\partial \sigma_{P_{R_i}}^2}{\partial r} \right)^2 \right], \quad (43)$$

where $\frac{\partial P_{R_i}}{\partial r}$ and $\frac{\partial \sigma_{P_{R_i}}^2}{\partial r}$ can be obtained from (40), i.e.,

$$\begin{cases} \frac{\partial P_{R_i}}{\partial r} = -P_t L(r, \theta_t, \theta_{r,i}) \left[\frac{1}{r} + \frac{k_e(\sin \theta_t + \sin \theta_{r,i})}{\sin(\theta_t + \theta_{r,i})} \right] \\ \frac{\partial \sigma_{P_{R_i}}^2}{\partial r} = -\frac{P_t L(r, \theta_t, \theta_{r,i}) h \nu}{T_d} \left[\frac{1}{r} + \frac{k_e(\sin \theta_t + \sin \theta_{r,i})}{\sin(\theta_t + \theta_{r,i})} \right]. \end{cases} \quad (44)$$

When the fluctuation of \hat{P}_{R_i} around P_{R_i} is small, \hat{r} can be regarded as an unbiased estimate of r . By defining $g(r, \theta_t, \theta_{r,i}) \triangleq \frac{1}{r} + \frac{k_e(\sin \theta_t + \sin \theta_{r,i})}{\sin(\theta_t + \theta_{r,i})}$, we can obtain the Cramér-Rao bound for estimating the distance r as

$$\text{Var}[r] \geq \frac{1}{\sum_{i=1}^N g^2(r, \theta_t, \theta_{r,i}) (P_t L(r, \theta_t, \theta_{r,i}) T_d / h \nu + \frac{1}{2})}. \quad (45)$$

From (45), we can observe that the Cramér-Rao bound for the estimating r will decrease as the number of receivers increases or the transmitting power P_t increases. Besides, we can also observe that the Cramér-Rao bound for the estimating r will increase as r increases.

TABLE I
SIMULATION PARAMETERS

Parameters	Value
$[r, \phi_r]$	[50 m, 0°]
$[\theta_T, \phi_T]$	[45°, 175°]
$[\theta_{R_1}, \theta_{R_2}, \theta_{R_3}]$	[40°, 50°, 60°]
$[\beta_t, \beta_r]$	[10°, 30°]
$[P_t, A_r]$	[100 mW, $1.77 \times 10^{-4} \text{ m}^2$]
$[k_a, k_s^{Ray}, k_s^{Mie}]$	[0.802, 0.266, 0.284] km ⁻¹
$[\gamma, g, f]$	[0.017, 0.72, 0.5]
d_0	2 m
σ_{ϕ_R}	1°
T_d	2/360 s
h	$6.626 \times 10^{-34} \text{ J}\cdot\text{s}$
c	$2.998 \times 10^8 \text{ m/s}$
λ	260 nm

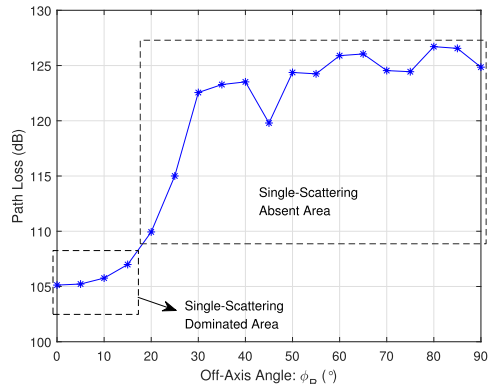


Fig. 3. Path loss under different off-axis angles ($\phi_T = 180^\circ$).

IV. NUMERICAL RESULTS

In this section, we present some numerical results to verify the performance of the proposed NLOS UV positioning method using linearly-arrayed photon-counting receivers. Unless otherwise specified, the parameters we adopt in this section are shown in Table I. We use the Monte-Carlo simulation to estimate the positioning errors and the biases of the proposed NLOS UV positioning methods. Here the positioning errors $\{e_{r_1}, e_{\phi_r}, e_{\theta_T}, e_{\phi_T}\}$ and biases $\{b_{r_1}, b_{\phi_r}, b_{\theta_T}, b_{\phi_T}\}$ are defined as the standard variance and the biases of the estimated $\{\hat{r}_1, \hat{\phi}_r, \hat{\theta}_T, \hat{\phi}_T\}$, i.e., $e_x \triangleq \sqrt{\frac{1}{M+1} \sum_{m=1}^M [\hat{x}(m) - \frac{1}{M} \sum_{m=1}^M \hat{x}(m)]^2}$ and $b_x \triangleq \frac{1}{M} \sum_{m=1}^M \hat{x}(m) - x$, where $\hat{x}(m)$ is the m th estimated value of x , M is the total sampling points of the Monte-Carlo simulation, and x is the real value. In this work, we set $M = 200$. The bias is an important metric here because we did not theoretically prove that all the estimators $\{\hat{r}_1, \hat{\phi}_r, \hat{\theta}_T, \hat{\phi}_T\}$ are unbiased estimators; and thus we have to check the bias using numerical results. The average calculating time for the proposed UV positioning methods with $d_0 \neq 0$ and $d_0 = 0$ are respectively 1.044 seconds and 2.749 seconds by using a computer with CPU clock speed of 3.2 GHz and memory of 16 GB, which are acceptable in practical systems.

We first present the path loss of the first three scattering orders obtained by Monte-Carlo simulation model [21] under different off-axis angles in Fig. 3. The path loss is defined as $10 \times \lg(P_t/P_r)$, where P_t and P_r are the transmitting power and the receiving power, respectively. When $\phi_T =$

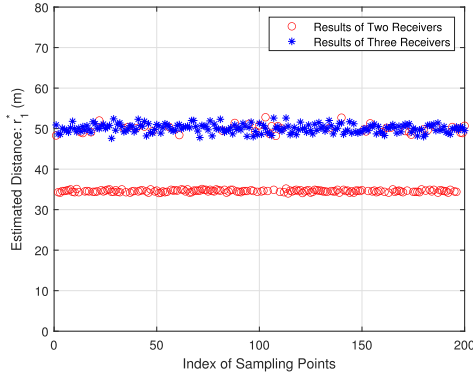
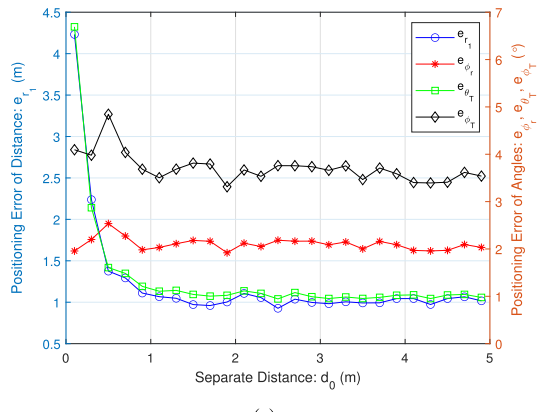
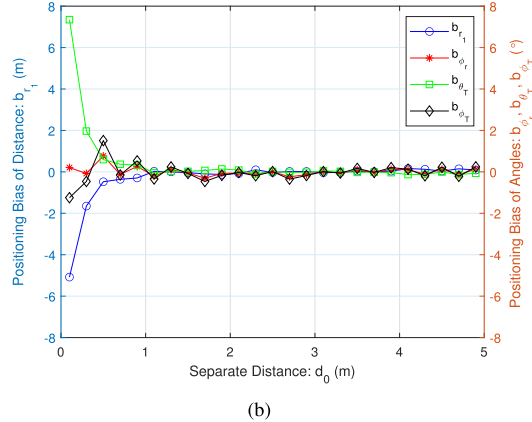


Fig. 4. Estimated distance r_1^* from two receivers with $[\theta_{R_1}, \theta_{R_2}] = [40^\circ, 60^\circ]$ and three receivers with $[\theta_{R_1}, \theta_{R_2}, \theta_{R_3}] = [40^\circ, 50^\circ, 60^\circ]$.



(a)

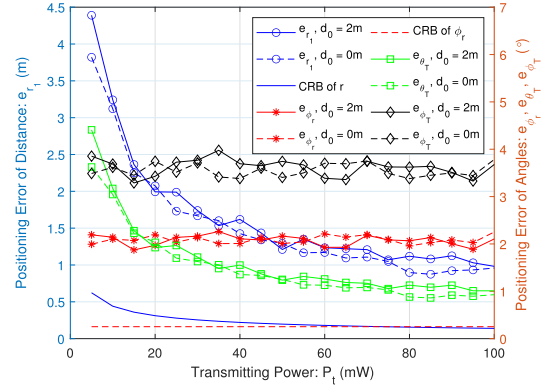


(b)

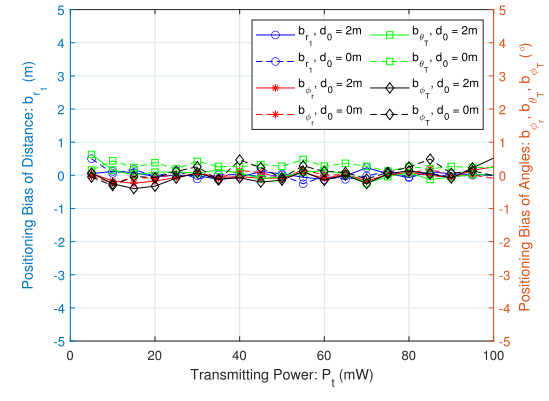
Fig. 5. The positioning error and bias performance under different separate distance: (a) positioning error $e_{r_1}, e_{\phi_r}, e_{\theta_T}$, and e_{ϕ_T} ; (b) positioning bias $b_{r_1}, b_{\phi_r}, b_{\theta_T}$, and b_{ϕ_T} .

180°, the off-axis angle is defined as the receiving azimuth angle ϕ_R . From Fig. 3, we can see that the path loss when the single-scattering is absent is much higher than that with single-scattering dominated case. Therefore, it is meaningful to maintain the single-scattering link between the transceivers by using the NLOS UV positioning methods.

We then present the estimated distance r_1^* from two receivers and three receivers in Fig. 4. From Fig. 4, we can see that there exists two possible solutions around 50 m and 35 m when only two receivers are employed. When three receivers are employed, only one possible solution around the true value 50 m is obtained. Therefore, three receivers can be used to avoid the multiple-solution problem.



(a)

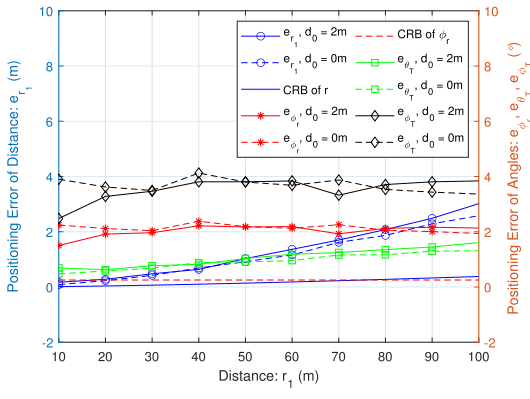


(b)

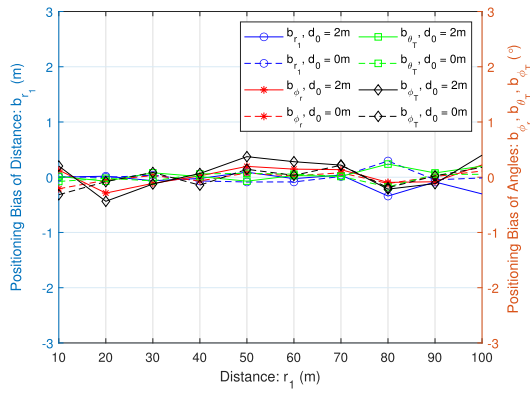
Fig. 6. The positioning error and bias performance under different transmitting power: (a) positioning error comparison between $d_0 = 2$ m and $d_0 = 0$ m; (b) positioning bias comparison between $d_0 = 2$ m and $d_0 = 0$ m.

Then we present the positioning error and bias under different separate distance d_0 in Figs. 5(a) and 5(b), respectively. The positioning error e_{r_1} and bias b_{r_1} of the distance are plotted on the left vertical axis and the positioning errors $\{e_{\phi_r}, e_{\theta_T}, e_{\phi_T}\}$ and biases $\{b_{\phi_r}, b_{\theta_T}, b_{\phi_T}\}$ are plotted on the right vertical axis. From Fig. 5(a) we can see that the positioning error of distance e_{r_1} decreases first fast then slowly as the separate distance d_0 increases. Besides, from Fig. 5(a), we can see that the positioning error for e_{ϕ_r} is around 2°, which is smaller than that obtained from a similar positioning method proposed in [54]. Similarly, from Fig. 5(b), we can also see that the positioning bias will approach zero fast as d_0 increases. When $d_0 \geq 2$ m, both the positioning error and the bias become stable. Therefore, we will adopt $d_0 = 2$ m in the following simulations. Besides, from Fig. 5(a) we can observe that $e_{\phi_T} > e_{\phi_r} > e_{\theta_T}$ when $d_0 \geq 2$ m. This indicates that it is more difficult to estimate the transmitting azimuth angle ϕ_T compared with the transmitting elevation angle θ_T .

Then we present the positioning error and bias under different transmitting power P_t in Figs. 6(a) and 6(b), respectively. The positioning errors and biases when $d_0 = 0$ are plotted for comparison. Besides, the square root of the Cramér-Rao bounds (CRBs) for estimating r and ϕ_r when $d_0 = 0$ are also plotted in Fig. 6(a). From Fig. 6(a), we can see that the gap between the proposed positioning method and the CRB is large, which means there is still a lot of room for improvement on the precision of NLOS UV positioning method. A large transmitting power can narrow the gap between the proposed



(a)



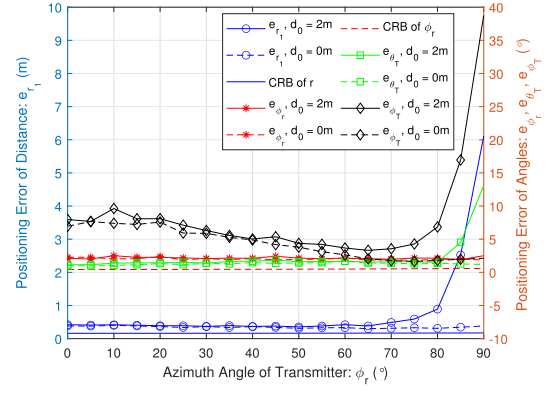
(b)

Fig. 7. The positioning error and bias performance under different communication distance: (a) positioning error comparison between $d_0 = 2$ m and $d_0 = 0$ m; (b) positioning bias comparison between $d_0 = 2$ m and $d_0 = 0$ m.

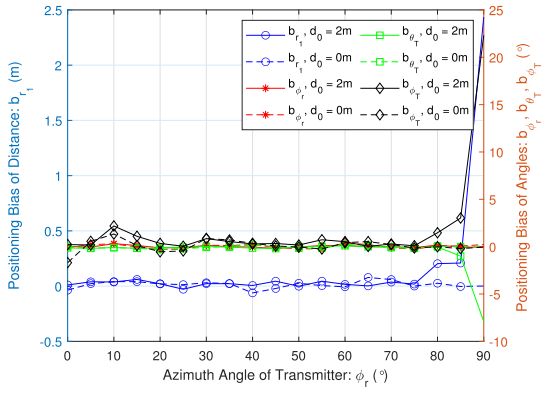
positioning method and the CRB. Besides, we can see that the positioning error of distance e_{r_1} decreases first fast then slowly as the transmitting power P_t increases. Therefore, we set $P_t = 100$ mW in the following simulations. From Fig. 6(b), we can see that the positioning biases for both $d_0 = 2$ m and $d_0 = 0$ m are small. Besides, similar to the results in Fig. 5(b), from Fig. 6(a) we can also observe that $e_{\phi_T} > e_{\phi_r} > e_{\theta_T}$ when $P_t \geq 20$ mW.

Then we investigate the positioning performance of the proposed NLOS UV positioning under different location parameters $\{r_1, \phi_r\}$ and pointing direction parameters $\{\theta_T, \phi_T\}$. Figs. 7(a) and 7(b) present the positioning error and bias under different distance r_1 , respectively. From Fig. 7(a), we can see that when r_1 is small, the positioning performance of r_1 is close to the CRB. However, the positioning error of distance e_{r_1} gradually increases as the distance r_1 increases; while the CRB only increases slowly. From Fig. 7(b), we can observe that the positioning bias for the azimuth angle b_{ϕ_r} of $d_0 = 0$ m is close to that of $d_0 = 2$ m.

Then we present the positioning error and bias under different azimuth angle of the transmitter ϕ_r in Figs. 8(a) and 8(b), respectively, where $\theta_T = 75^\circ$. From Fig. 8(a) we can see that the positioning errors when $d_0 = 2$ m will become large as ϕ_r approaches 90° , which corresponds to the case that the transmitter locating in the same line with N receivers. By contrast, the positioning errors when $d_0 = 0$ m



(a)



(b)

Fig. 8. The positioning error and bias performance under different azimuth angle of the transmitter: (a) positioning error comparison between $d_0 = 2$ m and $d_0 = 0$ m; (b) positioning bias comparison between $d_0 = 2$ m and $d_0 = 0$ m.

are much stable compared with those when $d_0 = 2$ m. From Fig. 8(b), we can see that although the positioning biases when $d_0 = 2$ m becomes large when ϕ_r approaches 90° , they are nearly zero when $\phi_r < 80^\circ$; whereas the biases b_{θ_T} and b_{ϕ_T} when $d_0 = 0$ m are stable as ϕ_r increases.

Then we present the positioning error and bias under different transmitting elevation angle θ_T in Figs. 9(a) and 9(b), respectively. From Fig. 9(a) we can see that the positioning errors of distance e_{r_1} are large when the transmitting elevation angle θ_T is small for both $d_0 = 2$ m and $d_0 = 0$ m; and when $\theta_T \geq 30^\circ$, we have $e_{r_1} \leq 2$ m. Besides, from both Figs. 9(a) and 9(b), we can see that when θ_T approaches 90° , both the positioning error e_{ϕ_T} and the bias b_{ϕ_T} will increase fast. This is because when θ_T is large, a small variation of the pointing direction will result in a large change on ϕ_T .

Then we present the positioning error and bias under different transmitting azimuth angle ϕ_T in Figs. 10(a) and 10(b), respectively, where $\theta_T = 75^\circ$. From Fig. 10(a) we can see that the positioning error e_{ϕ_T} becomes large when ϕ_T is close to 180° . From Fig. 10(b), we can see that the biases b_{ϕ_T} becomes large as ϕ_T approaches 180° for $d_0 = 0$ m.

Next we consider the impact of different receivers. The receiving elevation angle of the i th receiver is set as $\theta_{R_i} = 40^\circ + \frac{i-1}{N-1} \times 20^\circ$. Figs. 11(a) and 11(b) present the positioning error and bias under different number of receivers $N \in \{2, 3, 4, 5\}$, respectively. From Figs. 11(a) and 11(b)

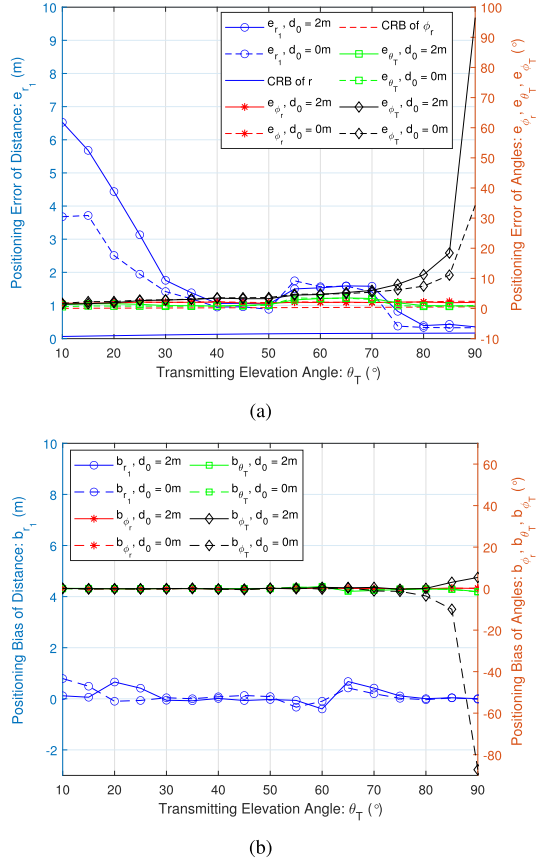


Fig. 9. The positioning error and bias performance under different transmitting elevation angle: (a) positioning error comparison between $d_0 = 2$ m and $d_0 = 0$ m; (b) positioning bias comparison between $d_0 = 2$ m and $d_0 = 0$ m.

we can observe that when $N = 2$, both the positioning errors and the biases are large due to the multiple-solution problem. As N increases from 2 to 3, the positioning errors and biases decrease fast to small values. However, we can also see that the positioning performance becomes stable when $N \geq 3$. Therefore, three receivers are enough for NLOS UV positioning method.

At last, we investigate the special case with $\theta_T = 90^\circ$. In this case, the receiver side only need to estimate the distance r_1 and the azimuth angle ϕ_r . The positioning error and bias under different separate distance d_0 are shown in Figs. 12(a) and 12(b), respectively. From Figs. 12(a) and 12(b), we can observe that the positioning performance is bad when d_0 is small. Besides, the positioning error will decrease first fast then slowly as the separate distance d_0 increases.

Combining the results from Fig. 4 to Fig. 12, we can obtain the following main observations:

- At least three receivers are needed to avoid multiple-solution problem of the proposed NLOS UV positioning method. Besides, three receivers are enough for achieving an acceptable positioning error of NLOS UV positioning method.
- The positioning error e_{r_1} of the proposed NLOS UV positioning method will decrease first fast then slowly as either the separate distance d_0 or the transmitting power P_t increases.
- The proposed NLOS UV positioning using linearly-arrayed photon-counting receivers can achieve a position-

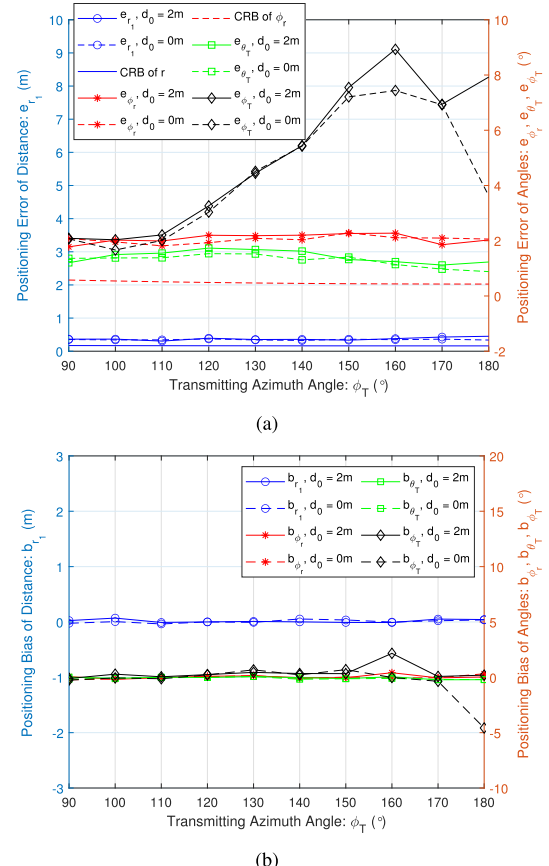


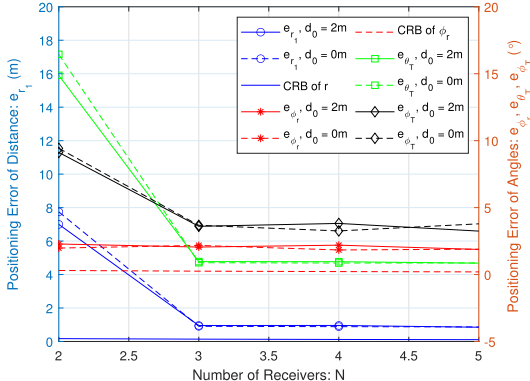
Fig. 10. The positioning error and bias performance under different transmitting azimuth angle: (a) positioning error comparison between $d_0 = 2$ m and $d_0 = 0$ m; (b) positioning bias comparison between $d_0 = 2$ m and $d_0 = 0$ m.

ing error less than 2 m when the transmitting elevation angle is greater than 30° and the separate distance is greater than 2 m.

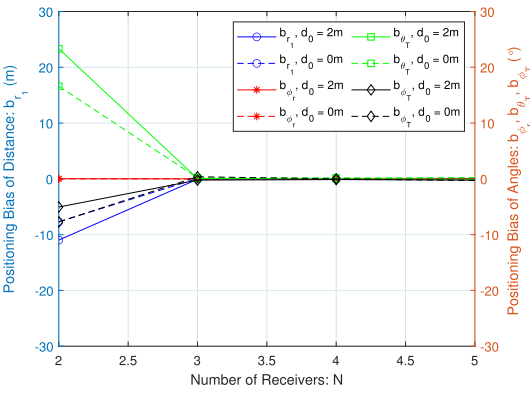
- The proposed UV portioning methods with $d_0 \neq 0$ m and $d_0 = 0$ m have their respective advantages. The positioning method with $d_0 \neq 0$ m can be used in cooperating positioning scenarios where each node has only one receiver with fixing receiving azimuth angle; whereas the positioning method with $d_0 = 0$ m can be used in independent positioning scenarios where each node can detect the UV signals at different receiving azimuth angles.

V. CONCLUSION

Traditional optical positioning techniques based on visible light signals or infrared light signals cannot be applied to NLOS positioning scenarios. In this work, we focus on NLOS UV positioning techniques using linearly-arrayed photon-counting receivers. We first established the geometrical and physical constraints for NLOS UV positioning techniques. Then we introduced two NLOS UV positioning methods using photon-counting receivers with the separate distance $d_0 \neq 0$ and $d_0 = 0$. Numerical results demonstrated that at least three receivers are required to avoid multiple-solution problem of the proposed NLOS UV positioning method; and three receivers are enough for achieving an acceptable positioning error of NLOS UV positioning method. Besides,



(a)

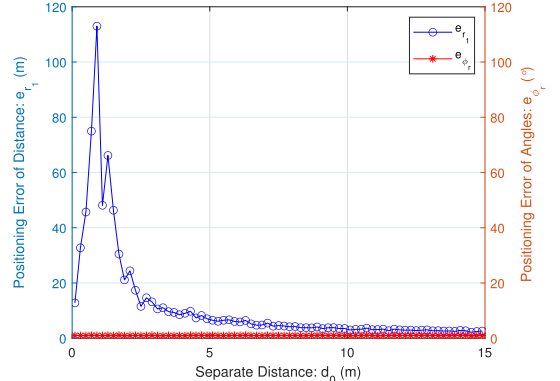


(b)

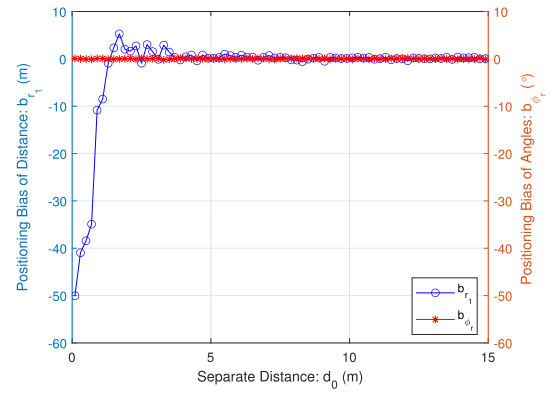
Fig. 11. The positioning error and bias performance under different number of receivers: (a) positioning error comparison between $d_0 = 2$ m and $d_0 = 0$ m; (b) positioning bias comparison between $d_0 = 2$ m and $d_0 = 0$ m.

we demonstrated that the positioning performance can be improved by increasing either the transmitting power or the separate distance. Moreover, we further demonstrated that the proposed NLOS UV positioning using linearly-arrayed photon-counting receivers can achieve a positioning error less than 2 m when the transmitting elevation angle is greater than 30° and the separate distance is greater than 2 m.

We would like to point out that the precision of the proposed UV positioning method is in meters, which is lower than the precision of VLP methods with centimeters. This is because the UV positioning is based on scattering effects of UV signals, where the information of the arriving angles and the arriving times are lost in the scattering process. Therefore, different from the VLP methods, the TOA or AOA based positioning methods cannot be directly applied to the NLOS UV positioning. This is also the reason why we designed UV positioning methods based on the receiving power in this work. Nevertheless, the precision in meters can still bring significant improvement on the link stability of practical UV communications because UV communications do not require strict alignment between the transceivers. Besides, the information of the relative arriving time of different photons is contained in the channel impulse response (CIR); and therefore it is reasonable to assume that CIR based positioning methods can achieve better positioning performance compared with receiving power based positioning methods. Therefore,



(a)



(b)

Fig. 12. The positioning error and bias performance under different separate distance when $\theta_T = 90^\circ$: (a) positioning errors e_{r_1} and e_{ϕ_r} ; (b) positioning biases b_{r_1} and b_{ϕ_r} .

in the future, we will explore the feasibility of NLOS UV positioning based on CIRs. Moreover, we will also explore the combined performance of both NLOS UV communication and UV positioning. In this context, this work sheds a light on designing NLOS UV communication systems with integrated communication and positioning functions.

APPENDIX

DERIVATION OF $l_{t,x}$, $l_{t,y}$, AND r_1 USING LEAST SQUARE METHOD

A. Derivation of $l_{t,x}$, $l_{t,y}$ in (14)

According to the least square method, we have $\mathbf{l} = (\mathbf{X}^T \mathbf{X})^{-1} \mathbf{X}^T \mathbf{y}$. We first obtain $\mathbf{X}^T \mathbf{X}$ as

$$\mathbf{X}^T \mathbf{X} = \begin{bmatrix} \sum_{i=1}^N \mu_{A_i, x}^2 & \sum_{i=1}^N \mu_{A_i, x} \mu_{A_i, y} \\ \sum_{i=1}^N \mu_{A_i, x} \mu_{A_i, y} & \sum_{i=1}^N \mu_{A_i, y}^2 \end{bmatrix}. \quad (46)$$

Then the inverse matrix of $\mathbf{X}^T \mathbf{X}$ can be obtained as

$$\begin{aligned} (\mathbf{X}^T \mathbf{X})^{-1} &= \frac{1}{|\mathbf{X}^T \mathbf{X}|} \begin{bmatrix} \sum_{i=1}^N \mu_{A_i, y}^2 & -\sum_{i=1}^N \mu_{A_i, x} \mu_{A_i, y} \\ -\sum_{i=1}^N \mu_{A_i, x} \mu_{A_i, y} & \sum_{i=1}^N \mu_{A_i, x}^2 \end{bmatrix}, \end{aligned} \quad (47)$$

where $|\mathbf{X}^T \mathbf{X}|$ is the determinant of matrix $\mathbf{X}^T \mathbf{X}$ and we have

$$|\mathbf{X}^T \mathbf{X}| = \left(\sum_{i=1}^N \mu_{A_i,x}^2 \right) \left(\sum_{i=1}^N \mu_{A_i,y}^2 \right) - \left(\sum_{i=1}^N \mu_{A_i,x} \mu_{A_i,y} \right)^2. \quad (48)$$

Besides, $\mathbf{X}^T \mathbf{y}$ can be obtained as

$$\mathbf{X}^T \mathbf{y} = \begin{bmatrix} -\sum_{i=1}^N \mu_{A_i,x} \mu_{A_i,z} \\ -\sum_{i=1}^N \mu_{A_i,y} \mu_{A_i,z} \end{bmatrix}. \quad (49)$$

Then after substituting (48) and (49) into \mathbf{l} , we can obtain $l_{t,x}$ and $l_{t,y}$ in (14).

Derivation of r_1 in (19)

Similarly, to derive r_1 , we can first rewrite the (18) as

$$\mathbf{S}r_1 = \mathbf{D}, \quad (50)$$

where $\mathbf{S} \triangleq [\sin(\phi_{R_1} - \phi_{R_2}), \sin(\phi_{R_1} - \phi_{R_3}), \dots, \sin(\phi_{R_1} - \phi_{R_N})]^T$ and $\mathbf{D} = [d_2 \cos \phi_{R_2}, d_3 \cos \phi_{R_3}, \dots, d_N \cos \phi_{R_N}]^T$.

Then using the least square method, we can obtain

$$\begin{aligned} r_1 &= (\mathbf{S}^T \mathbf{S})^{-1} \mathbf{S}^T \mathbf{D} \\ &= \frac{\sum_{i=2}^N d_i \cos \phi_{R_i} \sin(\phi_{R_1} - \phi_{R_i})}{\sum_{i=2}^N \sin^2(\phi_{R_1} - \phi_{R_i})}. \end{aligned} \quad (51)$$

REFERENCES

- [1] A. Jovicic, J. Li, and T. Richardson, "Visible light communication: Opportunities, challenges and the path to market," *IEEE Commun. Mag.*, vol. 51, no. 12, pp. 26–32, Dec. 2013.
- [2] W. Xu, J. Wang, H. Shen, H. Zhang, and X. You, "Indoor positioning for multiphotodiode device using visible-light communications," *IEEE Photon. J.*, vol. 8, no. 1, pp. 1–11, Feb. 2016.
- [3] J. Armstrong, Y. A. Sekercioglu, and A. Neild, "Visible light positioning: A roadmap for international standardization," *IEEE Commun. Mag.*, vol. 51, no. 12, pp. 68–73, Dec. 2013.
- [4] Y. Yang et al., "Positioning using wireless networks: Applications, recent progress and future challenges," 2024, *arXiv:2403.11417*.
- [5] F. Liu et al., "Survey on WiFi-based indoor positioning techniques," *IET Commun.*, vol. 14, no. 9, pp. 1372–1383, Jun. 2020.
- [6] D. Ko, M. Kim, K. Son, and D. Han, "Passive fingerprinting reinforced by active radiomap for WLAN indoor positioning system," *IEEE Sensors J.*, vol. 22, no. 6, pp. 5238–5247, Mar. 2022.
- [7] P. Davidson and R. Piché, "A survey of selected indoor positioning methods for smartphones," *IEEE Commun. Surveys Tuts.*, vol. 19, no. 2, pp. 1347–1370, 2nd Quart., 2016.
- [8] H. Xu, Y. Sun, Y. Zhao, M. Peng, and S. Zhang, "Joint beam scheduling and beamforming design for cooperative positioning in multi-beam LEO satellite networks," *IEEE Trans. Veh. Technol.*, vol. 73, no. 4, pp. 5276–5287, Apr. 2024.
- [9] Z. Xu and B. M. Sadler, "Ultraviolet communications: Potential and state-of-the-art," *IEEE Commun. Mag.*, vol. 46, no. 5, pp. 67–73, May 2008.
- [10] R. Yuan and J. Ma, "Review of ultraviolet non-line-of-sight communication," *China Commun.*, vol. 13, no. 6, pp. 63–75, Jun. 2016.
- [11] R. J. Drost and B. M. Sadler, "Survey of ultraviolet non-line-of-sight communications," *Semicond. Sci. Technol.*, vol. 29, no. 8, Jun. 2014, Art. no. 084006.
- [12] M. J. Weisman, F. T. Dagefu, T. J. Moore, C. H. Arslan, and R. J. Drost, "Analysis of the low-probability-of-detection characteristics of ultraviolet communications," *Opt. Exp.*, vol. 28, no. 16, pp. 23640–23651, Aug. 2020.
- [13] Y. Wang, C. Yang, Z. Ren, Y. Sun, and M. Peng, "Sensing-aided hybrid precoding for efficient terahertz wideband communications in multiuser high-data-rate IoT," *IEEE Internet Things J.*, vol. 11, no. 5, pp. 8253–8267, Mar. 2024.
- [14] Z. Liu, C. Yang, Y. Sun, and M. Peng, "Closed-form model for performance analysis of THz joint radar-communication systems," *IEEE Trans. Wireless Commun.*, vol. 22, no. 12, pp. 8694–8706, Dec. 2023.
- [15] Y. Ghasempour, Y. Amarasinghe, C.-Y. Yeh, E. Knightly, and D. M. Mittleman, "Line-of-sight and non-line-of-sight links for dispersive terahertz wireless networks," *APL Photon.*, vol. 6, no. 4, pp. 1–8, Apr. 2021, Art. no. 041304.
- [16] P. Mugen, Y. Renzhi, W. Zhifeng, and W. Siming, "Ultraviolet communication: Principle, techniques, and prospects," *J. Beijing Univ. Posts Telecommun.*, vol. 45, no. 3, pp. 13–18, Jun. 2022.
- [17] M. R. Luettgen, J. H. Shapiro, and D. M. Reilly, "Non-line-of-sight single-scatter propagation model," *J. Opt. Soc. Amer. A, Opt. Image Sci.*, vol. 8, no. 12, pp. 1964–1972, 1991.
- [18] Y. Zuo, H. Xiao, J. Wu, Y. Li, and J. Lin, "A single-scatter path loss model for non-line-of-sight ultraviolet channels," *Opt. Exp.*, vol. 20, no. 9, pp. 10359–10369, Apr. 2012.
- [19] T. Wu, J. Ma, P. Su, R. Yuan, and J. Cheng, "Modeling of short-range ultraviolet communication channel based on spherical coordinate system," *IEEE Commun. Lett.*, vol. 23, no. 2, pp. 242–245, Feb. 2019.
- [20] T. Wu, J. Ma, R. Yuan, P. Su, and J. Cheng, "Single-scatter model for short-range ultraviolet communication in a narrow beam case," *IEEE Photon. Technol. Lett.*, vol. 31, no. 3, pp. 265–268, Feb. 1, 2019.
- [21] R. J. Drost, T. J. Moore, and B. M. Sadler, "UV communications channel modeling incorporating multiple scattering interactions," *J. Opt. Soc. Amer. A, Opt. Image Sci.*, vol. 28, no. 4, pp. 686–695, 2011.
- [22] R. Yuan, J. Ma, P. Su, and Z. He, "An integral model of two-order and three-order scattering for non-line-of-sight ultraviolet communication in a narrow beam case," *IEEE Commun. Lett.*, vol. 20, no. 12, pp. 2366–2369, Dec. 2016.
- [23] R. Yuan, J. Ma, P. Su, Y. Dong, and J. Cheng, "An importance sampling method for Monte-Carlo integration model for ultraviolet communication," in *Proc. Int. Conf. Adv. Commun. Technol. Netw. (CommNet)*, Apr. 2019, pp. 1–6.
- [24] R. Yuan, J. Ma, P. Su, Y. Dong, and J. Cheng, "Monte-carlo integration models for multiple scattering based optical wireless communication," *IEEE Trans. Commun.*, vol. 68, no. 1, pp. 334–348, Jan. 2020.
- [25] T. Shan, R. Yuan, N. He, and J. Cheng, "Non-line-of-sight ultraviolet transmission coverage in non-precipitating, foggy, and rainy weather," *Opt. Exp.*, vol. 31, no. 23, pp. 37703–37721, Oct. 2023.
- [26] M. A. El-Shimy and S. Hranilovic, "Binary-input non-line-of-sight solar-blind UV channels: Modeling, capacity and coding," *J. Opt. Commun. Netw.*, vol. 4, no. 12, pp. 1008–1017, Dec. 2012.
- [27] M. A. El-Shimy and S. Hranilovic, "On the use of photon arrival-times for non-line-of-sight solar-blind UV channels," *IEEE Commun. Lett.*, vol. 18, no. 6, pp. 913–916, Jun. 2014.
- [28] Z. Wang, R. Yuan, and M. Peng, "Inter-symbol interferences deteriorated ultraviolet communications using photon-counting receivers," *IEEE Trans. Wireless Commun.*, vol. 23, no. 5, pp. 4097–4113, May 2024.
- [29] C. Gong and Z. Xu, "Channel estimation and signal detection for optical wireless scattering communication with inter-symbol interference," *IEEE Trans. Wireless Commun.*, vol. 14, no. 10, pp. 5326–5337, Oct. 2015.
- [30] C. Gong, X. Zhang, Z. Xu, and L. Hanzo, "Optical wireless scattering channel estimation for photon-counting and photomultiplier tube receivers," *IEEE Trans. Commun.*, vol. 64, no. 11, pp. 4749–4763, Nov. 2016.
- [31] Z. Wang, R. Yuan, M. Peng, S. Wang, X. Chu, and S. Di, "Full-duplex relay for ultraviolet communications using photomultiplier tube receivers," in *Proc. IEEE/CIC Int. Conf. Commun. China (ICCC)*, Aug. 2023, pp. 1–6.
- [32] Y. Zhang, C. Gong, and Z. Xu, "Bi-directional ultra-violet communication with self-interference," *Opt. Exp.*, vol. 30, no. 21, pp. 38534–38549, Oct. 2022.
- [33] Z. Wang, R. Yuan, and M. Peng, "Non-line-of-sight full-duplex ultraviolet communications under self-interference," *IEEE Trans. Wireless Commun.*, vol. 22, no. 11, pp. 7775–7788, Nov. 2023.
- [34] S. Wang, M. Peng, and R. Yuan, "MIMO free-space optical communications using photon-counting receivers under weak links," *IEEE Commun. Lett.*, vol. 27, no. 4, pp. 1185–1189, Apr. 2023.
- [35] R. Yuan and M. Peng, "Single-input multiple-output scattering based optical communications using statical combining in turbulent channels," *IEEE Trans. Wireless Commun.*, vol. 23, no. 4, pp. 2560–2574, Apr. 2024.
- [36] H. Qin, Y. Zuo, F. Li, R. Cong, L. Meng, and J. Wu, "Noncoplanar geometry for mobile NLOS MIMO ultraviolet communication with linear complexity signal detection," *IEEE Photon. J.*, vol. 9, no. 5, pp. 1–12, Oct. 2017.

- [37] X. Meng, M. Zhang, D. Han, L. Song, and P. Luo, "Experimental study on 1×4 real-time SIMO diversity reception scheme for a ultraviolet communication system," in *Proc. 20th Eur. Conf. Netw. Opt. Commun. (NoC)*, Jun. 2015, pp. 1–4.
- [38] G. Wang, K. Wang, C. Gong, D. Zou, Z. Jiang, and Z. Xu, "A 1 Mbps real-time NLOS UV scattering communication system with receiver diversity over 1 km," *IEEE Photon. J.*, vol. 10, no. 2, pp. 1–13, Apr. 2018.
- [39] L. Zhang, Z. Sun, T. Bai, P. Li, and Y. Qin, "1Mbps NLOS solar-blind ultraviolet communication system based on UV-LED array," in *Proc. Int. Conf. Opt. Instrum. Technol., Optoelectronic Devices Opt. Signal Process.*, Jan. 2018, Paper no. 106170O.
- [40] O. Alkhazragi et al., "Gbit/s ultraviolet-C diffuse-line-of-sight communication based on probabilistically shaped DMT and diversity reception," *Opt. Exp.*, vol. 28, no. 7, pp. 9111–9122, 2020.
- [41] T. Q. Wang, Y. A. Sekercioglu, A. Neild, and J. Armstrong, "Position accuracy of time-of-arrival based ranging using visible light with application in indoor localization systems," *J. Lightw. Technol.*, vol. 31, no. 20, pp. 3302–3308, Oct. 15, 2013.
- [42] S.-Y. Jung, S. Hann, and C.-S. Park, "TDOA-based optical wireless indoor localization using LED ceiling lamps," *IEEE Trans. Consum. Electron.*, vol. 57, no. 4, pp. 1592–1597, Nov. 2011.
- [43] B. Zhu, Z. Zhang, J. Dang, L. Wu, and L. Wang, "Low-complexity visible light positioning and rotation estimation based on eigenvalue decomposition," *J. Lightw. Technol.*, vol. 40, no. 21, pp. 7072–7083, Nov. 1, 2022.
- [44] N. Huang, C. Gong, J. Luo, and Z. Xu, "Design and demonstration of robust visible light positioning based on received signal strength," *J. Lightw. Technol.*, vol. 38, no. 20, pp. 5695–5707, Oct. 15, 2020.
- [45] N. Stevens, "Bias introduced by true radiation patterns in RSS-based visible light positioning," in *Proc. IEEE SENSORS*, Oct. 2019, pp. 1–4.
- [46] L. Bai, Y. Yang, C. Guo, C. Feng, and X. Xu, "Camera assisted received signal strength ratio algorithm for indoor visible light positioning," *IEEE Commun. Lett.*, vol. 23, no. 11, pp. 2022–2025, Nov. 2019.
- [47] Q. Liang, Y. Sun, L. Wang, and M. Liu, "A novel inertial-aided visible light positioning system using modulated LEDs and unmodulated lights as landmarks," *IEEE Trans. Autom. Sci. Eng.*, vol. 19, no. 4, pp. 3049–3067, Oct. 2022.
- [48] B. Zhu, J. Cheng, Y. Wang, J. Yan, and J. Wang, "Three-dimensional VLC positioning based on angle difference of arrival with arbitrary tilting angle of receiver," *IEEE J. Sel. Areas Commun.*, vol. 36, no. 1, pp. 8–22, Jan. 2018.
- [49] H. He, X. Ke, T. Zhao, and Y. Feng, "Research of position in the wireless 'solar-blind' ultraviolet mesh networks," *Laser Technol.*, vol. 34, no. 5, pp. 607–610, Sep. 2010.
- [50] T. Zhao, Y. Yu, H. Bao, and P. Song, "Ranging and positioning method using wireless solar blind ultraviolet," *Opt. Precis. Eng.*, vol. 25, no. 9, pp. 2324–2332, Sep. 2017.
- [51] Y. Li, L. Wang, Z. Xu, and S. V. Krishnamurthy, "Neighbor discovery for ultraviolet ad hoc networks," *IEEE J. Sel. Areas Commun.*, vol. 29, no. 10, pp. 2002–2011, Dec. 2011.
- [52] L. Wang, Y. Li, Z. Xu, and S. V. Krishnamurthy, "A novel neighbor discovery protocol for ultraviolet wireless networks," in *Proc. 14th ACM Int. Conf. Model., Anal. Simul. Wireless Mobile Syst.*, 2011, pp. 135–142.
- [53] Y. Zhao, Y. Zuo, H. Qin, X. Zhang, Q. An, and J. Wu, "A neighbor discovery protocol in ultraviolet wireless networks," in *Proc. Asia Commun. Photon. Conf. (ACP)*, Nov. 2014, pp. 1–3.
- [54] H. Qi, C. Gong, and Z. Xu, "Omnidirectional antenna array-based transmitter direction sensing in ultra-violet ad-hoc scattering communication networks," in *Proc. IEEE Int. Conf. Commun. Workshops (ICC Workshops)*, May 2019, pp. 1–6.
- [55] S. Wang et al., "Non-line-of-sight ultraviolet positioning using two photon-counting receivers," in *Proc. IEEE Global Commun. Conf. (GLOBECOM)*, Dec. 2023, pp. 1–5.
- [56] Å. Björck, "Least squares methods," *Handbook of Numerical Analysis*, vol. 1. Amsterdam, The Netherlands: Elsevier, Jan. 1990, pp. 465–652.
- [57] Z. Xu, H. Ding, B. M. Sadler, and G. Chen, "Analytical performance study of solar blind non-line-of-sight ultraviolet short-range communication links," *Opt. Lett.*, vol. 33, no. 16, pp. 1860–1862, 2008.
- [58] A. Ly, M. Marsman, J. Verhagen, R. P. P. P. Grasman, and E.-J. Wagenmakers, "A tutorial on Fisher information," *J. Math. Psychol.*, vol. 80, pp. 40–55, Oct. 2017.



Renzhi Yuan (Member, IEEE) received the B.S. degree in mechanical engineering from Tongji University, Shanghai, China, in 2011, the M.S. degree in precision instrument from Tsinghua University, Beijing, China, in 2017, and the Ph.D. degree in electrical engineering from The University of British Columbia, Kelowna, BC, Canada, in 2021. He is currently a Distinguished Research Fellow with the School of Information and Communication Engineering and the State Key Laboratory of Networking and Switching Technology, Beijing University of Posts and Telecommunications. His research interests include space-air-ground integrated communications, wireless optical communications, and quantum communications.



Siming Wang received the B.S. degree in communication engineering from Northeast University, Shenyang, China, in 2021. He is currently pursuing the Ph.D. degree with the School of Information and Communication Engineering and the State Key Laboratory of Networking and Switching Technology, Beijing University of Posts and Telecommunications. His research interests include wireless optical communications and machine learning.



Gang Liu is currently pursuing the B.S. degree in telecommunication engineering from Beijing University of Posts and Telecommunications, Beijing, China. His research interests include wireless optical communications and signal processing.



Mugen Peng (Fellow, IEEE) received the Ph.D. degree in communication and information systems from Beijing University of Posts and Telecommunications (BUPT), Beijing, China, in 2005. He joined BUPT, where he has been the Dean of the School of Information and Communication Engineering since June 2020 and the Deputy Director of the State Key Laboratory of Networking and Switching Technology since October 2018. In 2014, he was an Academic Visiting Fellow with Princeton University, USA. He has authored and coauthored over 150 refereed IEEE journal articles and over 250 conference proceedings papers. His research interests include wireless communication theory, radio signal processing, cooperative communication, self-organization networking, cloud communication, and the Internet of Things. He was a recipient of the 2018 Heinrich Hertz Prize Paper Award; the 2014 IEEE ComSoc AP Outstanding Young Researcher Award; and the Best Paper Awards in the IEEE ICC 2022, JCN 2016, IEEE WCNC 2015, IEEE GameNets 2014, IEEE CIT 2014, ICCTA 2011, IC-BNMT 2010, and IET CCWMC 2009. He is on the editorial/associate editorial board of *IEEE Communications Magazine*, *IEEE INTERNET OF THINGS JOURNAL*, *IEEE TRANSACTIONS ON VEHICULAR TECHNOLOGY*, and *IEEE TRANSACTIONS ON NETWORK SCIENCE AND ENGINEERING*.